Scientific report; WR-2000-02

KNMI

On the air-sea coupling in the WAM wave model

D.F. Doortmont and V.K. Makin

Koninklijk Nederlands Meteorologisch Instituut

De Bilt, 2000

Scientific report = Wetenschappelijk rapport; WR 2000-02

De Bilt, 2000

PO Box 201
3730 AE De Bilt
Wilhelminalaan 10
Telephone +31 30 220 69 11
Telefax +31 30 221 04 07

Authors: D.F. Doortmont and V.K. Makin

UDC: 551.526.63
551.466.33

ISSN: 0169-1651

ISBN: 90-369-2174-0

On the Air-Sea Coupling in the WAM Wave Model

D.F. Doortmont and V.K. Makin

Royal Netherlands Meteorological Institute (KNMI)
De Bilt, The Netherlands

Abstract

Wind generates waves on the surface of the ocean. Modifications of the sea state influence the wind profile just above it. The current WAM wave model, Cycle 4, incorporates the coupling back of the waves to the wind by modifying the Charnock constant by a coupling parameter defined as the ratio of the wave-induced stress to the total momentum flux. Shortcomings of the numerical implementation of the coupling are discussed. This coupling module is compared to one using a fixed Charnock constant which is shown to produce equally accurate significant wave heights. An alternative air-sea coupling parameterization is put forward, replacing the present wind input source function in the WAM model. It uses recently developed physics to calculate the momentum fluxes directly, without applying a Charnock type relation. A more accurate pre-described high-frequency tail of the wave spectrum is used to calculate the wave-induced stress. An iterative parameter tuning method is presented to estimate control parameters occurring in the air-sea coupling modules. It minimizes a cost-function representing the modelling error using a finite difference approach together with the Levenberg-Marquardt optimization method. Model experiments are performed for the North Sea to tune, validate and intercompare the alternative wind-wave coupling parameterizations in the WAM model. The impact on calculated wave parameters like significant wave height is studied.

Contents

1 Introduction

Atmospheric and ocean circulation systems are strongly influenced by processes occurring at the air-sea interface, concerning the exchange fluxes of momentum, heat, moisture and gasses in particular. These air-sea interaction processes are still not clearly understood and they give rise to uncertainties in weather prediction and climate change models that dynamically couple the two systems.

Wind generates waves on the surface of the ocean, while modifications of the sea state influence the wind profile just above it. The current research concentrates on modelling the interactive momentum exchange fluxes between the wind and the sea surface. Several alternative air-sea coupling modules are discussed and intercompared by their introduction into the WAve prediction Model (WAM) presented by Komen *et al.* (1994). The objective is to gain more insight into the influence of the physical and numerical parameterization of the coupling module on wave related processes, which can be used for recommending an air-sea interaction parameterization to incorporate into the coupling module of (operational) models like the WAM model or the European Coupled Atmosphere-Wave Ocean Model (ECAWOM). The ECAWOM model couples the two systems dynamically, see Weisse *et al.* (1997), which allows to study the effect of the coupling parameterizations on atmospheric processes likewise.

The currently widely used operational WAM wave prediction model, version Cycle 4, applies the air-sea coupling module developed by Janssen (1989, 1991). It incorporates the coupling back of the waves to the wind by dynamically modifying the Charnock parameter, which represents the proportionality between the roughness length and the stress of the sea surface, according to the sea state. The Charnock parameter is assumed to depend on a coupling parameter defined as the ratio of the wave-induced stress to the total momentum flux. This coupling parameter depends on the full wave spectrum, which makes it difficult to implement by a numerical scheme. The current research shows inconsistenties between theory and numerical implementation of the coupling parameter in the WAM Cycle 4 model, implying that the wind and waves are numerically not fully dynamically coupled. Another shortcoming of the air-sea parameterization in the WAM Cycle 4 model is the application of a rough approximation of the pre-described high-frequency tail of the wave spectrum by Phillips (1958), as described in e.g. WMO (1998). The modelling of developing wind sea requires a more accurate approximation of this diagnostic tail.

The effect of the coupling parameter on the calculated wave parameters is assessed in this report by comparing the output obtained by the WAM Cycle 4 model to that obtained by the WAM model using a fixed Charnock parameter, or equivalentely, a zero coupling parameter, in the Charnock relation. This alternative air-sea interaction parameterization, which is also used in WAMDI (1988), is less sophisticated than the coupling module applied in the WAM Cycle 4 model as it does not incorporate the influence of the sea state to the air flow just above the surface. The numerical implementation is therefore straightforward.

An alternative air-sea coupling parameterization is put forward, based on recently developed physics by Makin, Kudryavtsev and Mastenbroek (1995) and Makin and Kudryavtsev (1999). It replaces the wave growth rate parameterization of Miles (1957), incorporated in the wind input source function in the WAM Cycle 4 model, by a modern advanced parameterization based on rapid distortion theory as presented by Belcher and Hunt (1993). In contrast to the present air-sea coupling module in the WAM Cycle 4 model, this new air-sea coupling module calculates the momentum fluxes directly, without applying a Charnock type relation using the artificial concept of roughness length. Besides that, an accurate numerical

parameterization of the pre-described high-frequency tail of the wave spectrum suggested by Elfouhaily *et al.* (1997) is considered, which is based on an emperical high-frequency spectrum designed for remote sensing applications. The numerical implementation of the new growth rate parameterization is consistent with the physical model and it fully couples the air and sea surface in a dynamical way. This new air-sea coupling scheme is coded and incorporated into the WAM Cycle 4 model, replacing the original wind input source function, and its effect on the calculated wave parameters is assessed in the current studies.

The modified wind input source functions of the alternative air-sea coupling modules have to be tuned to the remaining source terms in the WAM model. Several control parameters are introduced in the models which are tuned by minimizing a certain cost-function, representing the misfit between the calculated WAM model output and the available wave observations. For this, an iterative parameter tuning method is developed and implemented. It applies a finite difference approximation together with the optimization method developed by Levenberg (1944) and Marquardt (1963), which efficiently combines the method of Newton and the method of steepest descent to approximate the minimum of the cost-function with respect to the control parameters. Each iteration step requires $M + 1$ WAM model runs together with the solution of a linear system of dimension M, where M is the number of control parameters, which is small in the current studies. The presented iteration algorithm of this robust and transparent tuning method is based on the one described by Press *et al.* (1992).

The parameter tuning method is applied to estimate several control parameters occurring in the Charnock relation and the dissipation source term of the original and modified WAM Cycle 4 model. This is performed for the North Sea area during a time period containing stormy as well as quiet weather. Fixed wind velocities obtained by an atmospheric model are used as input fields. Model experiments are executed using the tuned air-sea parameterizations to validate the wave model output against available North Sea buoy wave observations. The performance of the alternative tuned schemes is assessed and intercompared, and the impact on the calculated significant wave height and peak frequency is investigated.

The research presented in this report comes within the framework of the EC-project entitled *Air-Sea Wave Processes in Climate Change Models* that forms part of the Air-Sea Processes, EC ENvironment and Climate Programme (ASPEN). It describes the work performed by KNMI for Work Package 3 concerning the incorporation, tuning and validation of various air-sea coupling parameterizations in the WAM wave model. Further co-operating participants in this EC-project originate from research centres CPR, Italy, JCMM, United Kningdom and GKSS, Germany. The overall objective of the ASPEN project is to contribute to the improvement in reliability of climate predictions by improving the dynamic coupling between atmosphere and ocean circulation models by taking forward advanced research on models for air-sea processes associated with ocean waves.

Section 2 of this report describes the physics and numerical implementation of three alternative air-sea coupling modules in the WAM wave model. Several advantages and shortcomings of each parameterization are discussed. The iterative parameter tuning algorithm based on the Levenberg-Marquardt optimization method is outlined in Section 3. Section 4 and the Appendix present the WAM model results obtained by the alternative coupling modules, together with a validation and intercomparison assessment.

2 Air-sea coupling in WAM wave model

The basic equations of the WAM wave model are described in detail in Komen *et al.* (1994), a short outline is presented in this section. Three different parameterizations of the air-sea coupling specified in the wind input source function of the WAM model are presented. Firstly, the original WAM Cycle 4 model is recalled, containing the coupling theory of Janssen (1989, 1991) modelling a fully coupled air-sea situation. The parameterization in which the sea state is not coupled back to the wind velocity field is presented by the uncoupled air-sea model. An alternative air-sea coupling parameterization is presented by Makin and Kudryavtsev (1999). This new module couples the wind and waves dynamically and it is outlined as an alternative parameterization of the wind input source term. Various advantages and shortcomings concerning the physics and the numerical implementation of these air-sea parameterizations are discussed.

2.1 WAM Cycle 4 wave model

The basic equations of the WAM Cycle 4 wave model are shortly recalled from Komen *et al.* (1994). It is a third generation wave prediction model, which incorporates the air-sea coupling theory of Janssen (1989, 1991) modelling a dynamical interaction between the sea state and the wind velocity field above the sea surface by introducing a coupling parameter in the so-called Charnock relation.

2.1.1 Basic equations of wave energy input

The WAM model calculates the evolution of a two-dimensional, in frequency and direction, ocean wave spectrum in space and time by solving the energy transport equation,

$$\frac{dF}{dt} + \frac{\partial}{\partial\phi}\left(\dot{\phi}F\right) + \frac{\partial}{\partial\lambda}\left(\dot{\lambda}F\right) + \frac{\partial}{\partial\theta}\left(\dot{\theta}F\right) = S, \tag{1}$$

where $F = F(f, \theta; \boldsymbol{x}, t)$ represents the spectral density for waves with frequency f and direction of propagation θ at location $\boldsymbol{x} = (\phi, \lambda)$ and at time t. The source term S is a function of $f, \theta, \boldsymbol{x}, t$ and F itself, and it is defined by a superposition of four source terms,

$$S = S_{\text{in}} + S_{\text{dis}} + S_{\text{bot}} + S_{\text{nl}}, \tag{2}$$

where S_{in} is the wind input, S_{dis} is the dissipation by white-capping, S_{bot} is the bottom dissipation and S_{nl} is the non-linear wave-wave interactions source term. The momentum exchange between the air and the sea is incorporated in the wind input source function S_{in}, whose parameterization implemented in the WAM Cycle 4 model is recalled more extensively below. The wind input source function will be replaced and compared to two alternative air-sea coupling schemes in the WAM model presented in the next sections. The modified wind-wave coupling modules will be tuned against the dissipation source term S_{dis} by using various integral wave parameters.

Wave energy input by wind. The wind input source term S_{in} in the WAM model describes the energy transfer from the surface wind to the waves, given by the quasi-linear relation

$$S_{\text{in}} = \gamma F, \tag{3}$$

where γ is the growth rate parameter of the waves. In the WAM Cycle 4 model, γ depends on the entire wave spectrum F in an implicit way, parameterized by the following set of equations.

The wind speed above the sea surface is represented by a logarithmic profile, originating from the integration of the momentum balance equation,

$$U(z) = \frac{u_*}{\kappa} \log\left(\frac{z}{z_0}\right) = \frac{u_*}{\sqrt{C_D(z)}}, \tag{4}$$

in which $U(z)$ is the wind velocity at height z, $\kappa = 0.41$ is the Von Karman constant, z_0 is the roughness parameter of the sea surface, u_* is the friction velocity and $C_D(z)$ is the drag coefficient at height z. The total air-sea momentum flux τ is a superposition of the height-dependent turbulent stress τ_t and the wave-induced stress τ_w, i.e. $\tau = \tau_t(z) + \tau_w(z)$, and friction velocity u_* is related to the surface stress τ by

$$\tau = \rho_a u_*^2, \tag{5}$$

where ρ_a is the density of the air. Total stress τ and friction velocity u_* are assumed to be independent of height. The friction velocity of the wind and the roughness length are coupled through the Charnock relation,

$$z_0 = \alpha \frac{u_*^2}{g}, \tag{6}$$

where proportionality parameter α is called the Charnock parameter. This relation was derived by Charnock (1955) and it is purely based on dimension analysis. Charnock (1955) assumes parameter $\alpha = \hat{\alpha}$ to be a given constant, implying that roughness length z_0, friction velocity u_* and drag coefficient C_D at height z can be derived by solving the implicit relations (4) and (6) for a given wind profile. In other words, a fixed constant α fully determines z_0, u_* and C_D by the assumed wind profile and the Charnock relation.

Experiments show however, see Janssen (1989, 1991), that the presence of waves also influences the wind profile near the sea surface, e.g. a rougher sea-surface slows down the air-flow just above it more than a flat sea-surface, implying that relation (4) breaks down near the sea-surface. This dynamical coupling back of the sea state to the wind profile is not modelled correctly by assuming a constant Charnock parameter α. In order to incorporate the coupling back, Janssen (1989, 1991) proposed a modification of wind profile (4) by using a variable Charnock parameter α depending dynamically on the sea state through the wave-induced stress $\tau_w = |\boldsymbol{\tau}_w|$. The components of the wave-induced surface stress vector $\boldsymbol{\tau}_w = (\tau_{w_1}, \tau_{w_2})$ depend on the complete wave spectrum F, by

$$\tau_{w_1} = \int_0^{\infty}\int_0^{2\pi} \omega\gamma F \sin\theta d\theta df, \qquad \tau_{w_2} = \int_0^{\infty}\int_0^{2\pi} \omega\gamma F \cos\theta d\theta df, \tag{7}$$

in which ω is the angular frequency and γF equals S_{in} of (3). According to the theory of Janssen (1989, 1991), the wave-dependent Charnock parameter α of relation (6) reads

$$\alpha = \frac{\hat{\alpha}}{\sqrt{1-y}}, \qquad \hat{\alpha} = 0.01, \tag{8}$$

where the so-called coupling parameter y is defined as the ratio of the wave-induced stress at height z_0 to the total momentum flux, i.e.

$$y = \frac{\tau_w}{\tau}. \tag{9}$$

This air-sea coupling parameterization is implemented in the WAM Cycle 4 model. It uses value $\hat{\alpha} = 0.01$, which is obtained by assuming $y = 0.71$ for a fully developed sea together with the commonly used Charnock constant $\alpha = 0.0185$ for old wind sea. For small y, the modified Charnock relation resembles the original one from Charnock (1955) using a constant parameter, whereas an enhanced wind stress is created when y approaches 1. Roughness parameter z_0, friction velocity u_* and drag coefficient C_D depend on both the assumed wind profile (4) and the ocean sea state F, through coupling parameter y of (9) in the Charnock relation (6).

The input for the wave model is the wind speed at 10 m height $U_{10} = U(10)$. Quantities u_* and z_0 are calculated from the implicit relations (4)-(9) for given U_{10} and τ_w. They determine on their turn growth rate γ according to the theory of Miles (1957), i.e.

$$\frac{\gamma}{\omega} = \frac{\rho_{\mathrm{a}}}{\rho_{\mathrm{w}}}\beta(x, z_0)x^2, \tag{10}$$

where ρ_{w} is the density of the sea water, and parameters $\beta = \beta(x, z_0)$ and x are defined by

$$x = \left(\frac{u_*}{c_p} + z_\alpha\right)\cos(\theta - \phi), \qquad \beta = \frac{\beta_m}{\kappa^2}\mu\log^4(\mu), \qquad \mu = \min\left\{\frac{gz_0}{c_p^2}e^{\kappa/x}, 1\right\}, \tag{11}$$

in which c_p is the phase speed of the waves at the peak of the spectrum, ϕ is the wind direction, $z_\alpha = 0.011$ is a tuned parameter, constant $\beta_m = 1.2$ determines the overall strength of S_{in} and $g = 9.81$ ms^{-2} is the gravitational acceleration. For a given spectrum F, equations (4)-(11) form a closed set of implicit equations, which is numerically solved by the WAM Cycle 4 model.

Wave energy dissipation. The source term S_{dis} in the WAM model represents the dissipation of wave energy by white-capping, given by

$$S_{\mathrm{dis}} = -C_{\mathrm{dis}}\langle\omega\rangle\left(\frac{\alpha}{\alpha_{\mathrm{PM}}}\right)^2\frac{k}{2\langle k\rangle}\left(1 + \frac{k}{\langle k\rangle}\right), \tag{12}$$

where k is the wave number, $\alpha_{\mathrm{PM}} = 4.57 \times 10^{-3}$ is the Pierson-Moskowitz steepness for a fully developed sea and $\alpha = E\langle k\rangle^2$ is the squared average steepness of the spectrum. Dimensionless constant $C_{\mathrm{dis}} = 9.4 \times 10^{-5}$ determines the overall strength of S_{dis}. The total wave variance E is defined by

$$E = \int_0^\infty\int_0^{2\pi} F(f, \theta)d\theta df, \tag{13}$$

and the mean angular frequency and mean wave number are defined, respectively, by

$$\langle\omega\rangle = E\left(\int_0^\infty\int_0^{2\pi} F(f, \theta)\omega^{-1}d\theta df\right)^{-1}, \qquad \langle k\rangle = E\left(\int_0^\infty\int_0^{2\pi} F(f, \theta)k^{-1/2}d\theta df\right)^{-2}. \tag{14}$$

Integral wave parameters. After solving the energy balance equation by the WAM model, various important integral wave parameters can be derived from the calculated spectra. The most commonly used are significant wave height H_s, defined by

$$H_s = 4\sqrt{E}, \tag{15}$$

and peak frequency f_p, defined as the frequency at the maximum of the one-dimensional wave spectrum,

$$F(f) = \int_0^{2\pi} F(f,\theta)d\theta, \tag{16}$$

Both H_s and f_p depend on place and time. They can be used for model verification and parameter estimation studies if observations are available.

2.1.2 Numerical implementation

Several aspects are discussed concerning the numerical implementation of the physics concerning, among other things, the air-sea coupling in the WAM Cycle 4 model as recalled in the former section. The numerical calculation of the coupling parameter is discussed, as well as the application of a pre-assumed high-frequency tail of the spectrum. Two limiters are mentioned which are introduced in the numerical model because of stability reasons.

Coupling parameter. Firstly, the numerical implementation of the wind input source term S_{in} in the WAM Cycle 4 model is discussed. For S_{in}, the WAM model uses an implicit second order centered difference model to discretize (1) with respect to time. The calculation of the increment of S_{in} from a certain time instant t_{old} to a time instant t_{new} at a specific location requires growth rate parameter γ at t_{new}, which in its turn requires u_* (and z_0) at t_{new} to evaluate (10)-(11).

The calculation of $u_*(t_{\text{new}})$ by solving the implicit set of equations (4)-(9) for a given wind input $U_{10}(t_{\text{new}})$ introduces a numerical difficulty because the full spectrum F at time t_{new} is required for τ_w of (7) to determine coupling parameter y of (9). Instead of solving this implicit set at each time instant, the following simplification is made in the numerical WAM model. Before performing the actual runs to integrate equation (1) numerically, the WAM Cycle 4 model pre-calculates a two-dimensional table containing the total surface stress $\tau = \tau[\tau_w, U_{10}]$ for a given discrete set of wave-induced stresses τ_w and wind velocities U_{10}. This table is constructed by taking a broad range of fixed values of U_{10} and τ_w for which the implicit non-linear set of equations (4)-(9), without (7), is solved iteratively by the method of Newton. For a given pair of τ_w and U_{10}, the corresponding approximation of τ is calculated by linear interpolation from this table.

The WAM Cycle 4 model calculates $\gamma(t_{\text{new}})$ numerically as follows. At time instant t_{new}, the WAM model approximates $\tau_w(t_{\text{new}})$ by $\tau_w(t_{\text{old}})$ which has already been calculated by evaluating integrals (7) during the previous time step. Coupling parameter y at t_{new} is approximated by y^*, given by

$$y^*(t_{\text{new}}) = \frac{\tau_w(t_{\text{old}})}{\tau^*}, \qquad \tau^* = \tau[\tau_w(t_{\text{old}}), U_{10}(t_{\text{new}})], \tag{17}$$

where τ^* is derived from the pre-calculated table of the total stress. After this, approximations to u_*, z_0 and γ are obtained at t_{new} by evaluating relations (5)-(11), without (7). This means that the numerical WAM Cycle 4 model does not fully dynamically couple the wind and the sea as described by the physics of Section 2.1.1.

Besides that, the WAM Cycle 4 model avoids the singularity caused by a possible division by zero in (8), by limiting the numerical coupling parameter. In other words, parameter

$$y^{\text{WAM}}(t_{\text{new}}) = \min\{y^*(t_{\text{new}}), 0.999\}, \tag{18}$$

is the actual numerical coupling parameter implemented in the WAM Cycle 4 model. This means that the numerical and physical model of the air-sea coupling parameterization are not fully consistent in WAM Cycle 4.

High-frequency tail. Another part of discussion is the application of the high-frequency tail introduced into the numerical WAM model to reduce computation time. The high-frequency part of the wave spectrum is important for calculating the momentum flux between the wind and the sea. It can be shown, see e.g. Makin and Kudryavtsev (1999), that the air-sea momentum exchange for developing wind waves takes place primarily at the high-frequency part of the spectrum, which therefore has to be modelled accurately.

The numerical WAM Cycle 4 model solves the energy balance equation (1) up to a certain dynamically determined cut-off frequency f_c, which is dependent on place, time, u_*, mean frequency of the spectrum, and largest frequency in the discrete frequency grid, as described by Burgers (1990). The low frequency part of the calculated wave spectrum F, i.e. for $f \leq f_c$, is called the prognostic part of the wave spectrum. Cut-off frequency f_c corresponds to a wave length $\lambda \approx 10$ m.

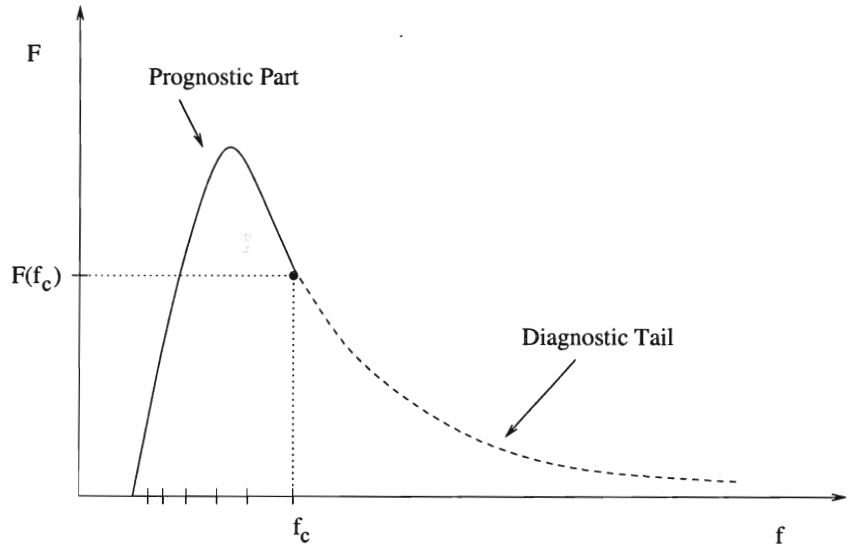

Figure 1: *Prognostic part and diagnostic high-frequency tail of wave spectrum F.*

For frequencies larger than f_c, i.e. for waves shorter than 10 m, the spectrum is assumed to behave according to a diagnostic tail, which is proportional to f^{-5} as described by Phillips (1958). In other words, the high-frequency part of spectrum F is assumed to be

$$F \sim f^{-5}, \qquad f \geq f_c, \tag{19}$$

where the proportionality constant equals $F(f_c)f_c^5$ patching the prognostic part to the diagnostic tail of the spectrum. Figure 1 schematically shows the prognostic and diagnostic part of a wave spectrum. The complete high-frequency tail is merely determined by cut-off frequency f_c, the pre-assumed f^{-5}-profile of the diagnostic tail and spectral level $F(f_c)$.

The prognostic part of the wave spectrum is dependent on the so-called inverse wave age, defined by ratio U_{10}/c_p, describing the stage of wave development for wind sea. This relation lifts the prognostic part of the spectrum upward for young sea, whereas it is pushed

downward for old sea. However, the high-frequency part of the spectrum is also shifted up- and downward according to patching spectral level $F(f_c)$ of the highest prognostic frequency bin by (19). This numerical feature implies a direct relation between the wave age and the high-frequency part of the wave spectrum, which does not correspond to the behaviour of the diagnostic tail observed in nature, see discussions in Makin, Kudryavtsev and Mastenbroek (1995) and Elfouhaily *et al.* (1997), which is a drawback of the application of the pre-described high-frequency tail.

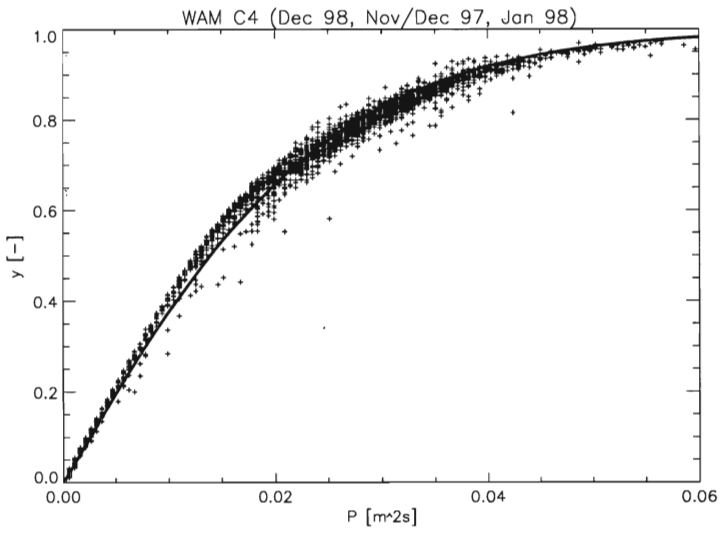

Figure 2: *Numerical coupling parameter y versus parameter P of (20), together with regression curve y^{reg} of (21), obtained by the WAM Cycle 4 model at observation stations AUK, EURO, K13 and IJM, for time periods Nov '97 - Jan '98 and Dec '98.*

The following is remarked with regard to the air-sea coupling parameter y and the high-frequency tail used in the WAM Cycle 4 model. A certain quantity P is considered, which is calculated by the WAM Cycle 4 model at time instant t_{new}, defined by

$$P = \int_0^{2\pi} F(f_m, \theta)\delta d\theta, \qquad f_m = 0.4117 \text{ Hz}, \tag{20}$$

where f_m is the maximum value of the discrete frequency grid, $\delta = \max\{\cos^3(\theta - \phi), 0\}$ and $F(f_m, \theta)$ is the value of wave spectrum F evaluated at f_m at the former time instant t_{old}. Model experiments have been performed using Wam Cycle 4 for the North Sea area during several independent time periods. The experimental set-up is described in detail in Section 4.1. Figure 2 shows the scatter plot of the numerical coupling parameter y of the WAM Cycle 4 model given by (18) versus quantity P. The model output at four observation stations during four months are displayed in this figure.

The little scatter shown in the plot of Figure 2 suggests a direct relationship between parameter P and the numerical coupling parameter in the WAM Cycle 4 model. This relationship can be parameterized e.g. by the non-linear regression curve y^{reg}, defined by

$$y^{\mathrm{reg}}(P) = \tanh(AP), \qquad A = 39.3. \tag{21}$$

Regression coefficient A is obtained by applying the method of least-squares together with the iterative method of Newton to minimize the sum of squared errors between the calculated coupling parameter and the corresponding value of the fitting curve y^{reg} with respect to A.

The scatter plot shows that coupling parameter y, at t_{new}, is determined by the wave spectrum F at only one frequency value $f_m = 0.4117$ Hz at the former time instant t_{old}. This means that the wind and the waves are not fully dynamically coupled in the numerical WAM Cycle 4 model. The application of the numerical coupling parameter y^{WAM} of (18) and the high-frequency f^{-5}-tail of (19) in the numerical WAM Cycle 4 model are not consistent with the physics of the wave model. Therefore, an alternative parameterizition of the wind-sea interaction is required.

Limiter. The last remark made in this section concerns a limiter introduced in the WAM model for numerical stability reasons. It limits the wave spectrum change, but it is not directly related to the parameterization of the air-sea interaction process. The discrete change of the wave spectrum $\Delta F = F(t_{\mathrm{new}}) - F(t_{\mathrm{old}})$ at time instant t_{new} is calculated by the integration of the total effective source term, i.e. $\Delta F = S(t_{\mathrm{old}})\Delta t$. In the WAM Cycle 4 model, this discrete change of F is restricted by a limiter. It limits each discrete spectral bin ΔF after an integration time step, by

$$\Delta F_{\mathrm{lim}}(t_{\mathrm{new}}) = \mathrm{sign}(S(t_{\mathrm{old}})) \min \{ \mid S(t_{\mathrm{old}}) \mid \Delta t, L \}, \tag{22}$$

where $\Delta F_{\mathrm{lim}} = F_{\mathrm{lim}}(t_{\mathrm{new}}) - F(t_{\mathrm{old}})$ is the restricted discrete maximum change of F per time step and limiter L is defined by

$$L = \tilde{L}\frac{\Delta t}{1200}, \qquad \tilde{L} = 0.62 \times 10^{-4} f^{-5} \ \mathrm{m^2 s^{-4}}. \tag{23}$$

Limiter L is applied after calculating the total effective source function S and before determining cut-off frequency f_c and adding the high-frequency f^{-5}-tail in each time step. Limiter L is frequency dependent restricting especially the absolute change of F for the high-frequency wave components up to the cut-off frequency. Restriction (22) on ΔF using limiter (23) is independent of Δt, implying that the relative impact of limiter L will not vanish for decreasing Δt. This means that the limiter becomes an integral part of the numerical solution which no longer converges to the solution for the physics parameterization of the model.

The overall impact of the limiter can be assessed by studying the ratio between the discrete spectral change after and before the limiter is applied, defined by

$$\varepsilon(t_{\mathrm{new}}) = \frac{\int_0^{f_c}\int_0^{2\pi} |\Delta F_{\mathrm{lim}}| d\theta df}{\int_0^{f_c}\int_0^{2\pi} |\Delta F| d\theta df}, \tag{24}$$

reflecting the total number of times limiter L is applied at time instant t_{new}. If $\varepsilon = 1$ the limiter is not applied, but smaller values of $\varepsilon < 1$ mean a larger impact of the limiter on the total spectral change. Ratio ε is assessed in the current studies.

2.2 Uncoupled air-sea wave model

The air-sea coupling module presented in this section applies a simpler air-sea coupling parameterization used in previous versions of the WAM Cycle 4 model, see e.g. WAMDI (1988), because it does not couple back the influence of the sea state on the wind profile above the

surface. The considered wave model is identical to WAM Cycle 4 presented in the previous section, except for the air-sea coupling parameterization of wind input source term S_{in}. One is referred to Section 2.1.1 for the basic equations of the model. As already mentioned, the WAM Cycle 4 model couples back the changing sea state to the wind profile by modifying Charnock parameter α in (6) in Charnock relation (8) by coupling parameter y of (9) according to the theory of Janssen (1989, 1991).

The air-sea coupling module considered in this section, however, adopts the idea originally presented in Charnock (1955). The Charnock parameter α in (6) is modelled by a given constant. In other words, the coupling parameter y defined in (9), or equivalently, the wave-induced stress τ_w, is assumed to be zero,

$$y = \frac{\tau_w}{\tau} = 0, \tag{25}$$

yielding, through (8), a constant Charnock parameter $\alpha = \hat{\alpha}$ in the Charnock relation defined by (6), i.e.

$$z_0 = \hat{\alpha}\frac{u_*^2}{g}. \tag{26}$$

It means that roughness parameter z_0, friction velocity u_* and drag coefficient C_D are determined by the logarithmic wind profile (4) and Charnock relation (26), which are independent of the sea state. This wave model containing the modified wind input source term without the back coupling of the waves to the air flow is referred to as the uncoupled air-sea model.

The wind input source term calculation in the uncoupled air-sea model is simpler than the calculation of S_{in} in the WAM Cycle 4 model. Roughness parameter z_0 and friction velocity u_* are iteratively determined from equations (4) and (26) for a given wind input field U_{10}, which does not require the full wave spectrum F to calculate stress τ_w. Note that comparison of the original WAM Cycle 4 model against this uncoupled air-sea model assesses the impact of coupling parameter y of (9) on the generated wave output.

2.3 New air-sea coupling module

An alternative physical parameterization of the air-sea coupling based on recent developments by Makin and Kudryavtsev (1999) is concisely described in this section. The basic equations are shortly outlined and several aspects are compared to the coupling module of the original WAM Cycle 4 model. This new wind input source term is introduced into the WAM Cycle 4 model, replacing the original parameterization. Its numerical implementation is shortly discussed.

2.3.1 New growth rate parameterization

The new air-sea coupling module concisely described in this section is based on the parameterization presented by Makin and Kudryavtsev (1999). The original WAM Cycle 4 model is considered except for the wind input source function S_{in} specified in Section 2.1.1. The growth rate γ of S_{in} as parameterized by (10) in the original WAM Cycle 4 model is replaced by a new parameterization,

$$S_{\text{in}} = \gamma F \quad \rightarrow \quad S_{\text{in}}^{\text{new}} = \gamma^{\text{new}} F, \tag{27}$$

where the new growth rate γ^{new} again depends on the entire specrum F in an implicit way by a closed set of equations presented below.

The velocity profile U of the wind above the waves as a function of height z is given by

$$U(z) = u_*^2 \int_0^z \left(1 - \frac{\tau_w(z')}{u_*^2}\right) (K + \nu)^{-1} \, dz', \tag{28}$$

which is obtained by integrating the momentum balance equation for the height-independent total stress $\tau = \tau_t(z) + \tau_w(z) + \tau_\nu(z) = u_*^2$, where τ_ν is the viscous stress in the boundary sublayer and $\nu = 10^{-5}$ m^{2}s^{-1} is the kinematic viscosity of the air. All stresses are normalized by ρ_a in this formulation. Coefficient $K(z)$ is the eddy-viscosity defined by

$$K = \kappa z u_* \left(1 - \frac{\tau_w(z)}{u_*^2}\right)^{1/4} d(z, u_*), \qquad d = 1 - e^{-z u_*/36\nu}, \tag{29}$$

where d is the damping function by Van Driest introduced to approximate the velocity profile within the molecular sublayer. It allows an explicit description of the stress behaviour within the viscous sublayer and avoids the application of the viscous roughness length concept applied by Makin and Kudryavtsev (1999).

The wave-induced stress τ_w is defined as a function of height z by the integral

$$\tau_w(z) = \int_0^\infty \mathcal{T}(k) e^{-z/\mathcal{L}} d(\log k), \tag{30}$$

where $\mathcal{L} = 1/5k$ is the height of the inner layer and $\mathcal{T}$ is the omni-directional spectrum of the momentum flux to the waves,

$$\mathcal{T}(k) = \int_{-\pi}^{\pi} c^2 B(k, \varphi) \beta(k, \varphi) \cos\varphi \, d\varphi, \tag{31}$$

in which c is the phase velocity, φ is the propagation direction of the k-wave component relative to the wave direction and $B(k, \varphi) = k^4 F(k, \varphi)$ is the saturation spectrum. Directional wave spectrum $F(k, \varphi)$ is described as a function of k and φ rather than f and θ in this formulation. The newly defined growth rate parameter is based on rapid distortion theory as presented by Belcher and Hunt (1993). It reads

$$\frac{\gamma^{\text{new}}}{\omega} = \frac{\rho_a}{\rho_w} \beta(k, \varphi), \tag{32}$$

where β describes the energy flux from the air to the waves by

$$\beta = m_\beta R \left(\frac{u_*}{c}\right)^2 \left(1 - y\overline{f}(k)\right) \cos\varphi \, |\cos\varphi|, \tag{33}$$

in which $m_\beta = 0.045$ according to Plant (1982) and coupling parameter $y = \tau_w(0)/u_*^2$ equals definition (9). The dimensionless wave-induced stress averaged over the surface boundary layer $\overline{f}$ is defined by

$$\overline{f}(k) = \frac{1}{\tau_w(0)} \int_0^\infty \tau_w(z) e^{-kz/k\delta} d(kz/k\delta), \tag{34}$$

where $\tau_w(z)$ is the form drag defined by (30), $\overline{f} \to 1$ for very short waves, while $\overline{f} \to 0$ for longer waves. Here $k\delta = 0.04$ and relaxation function R is defined by

$$R = 1 - 0.3 \left(\frac{c}{U_{10}}\right)^5, \tag{35}$$

yielding $R \sim 1$ for slowly moving waves, while $R \to 0$ for fast moving waves. It is assumed that the growth rate equals zero when $R < 0$, i.e. for waves moving faster than the wind.

It is emphasized that the new parameterization of the air-sea coupling calculates the momentum fluxes between the wind and the waves directly. As opposed to the air-sea coupling parameterization in the original WAM Cycle 4 model, the artificial concept of roughness length and the pre-described Charnock relation are not used in this model. Instead of applying the theory of Miles (1957) to model the growth rate, the new parameterization is based on rapid distortion theory by Belcher and Hunt (1993). The wind profile and the state of the sea surface are fully coupled in a dynamical way.

For a given spectrum F, equations (28)-(35) form a closed implicit set, which is solved iteratively. Just like the WAM Cycle 4 model, it requires the full wave spectrum to determine the stress. The next section describes the numerical implementation of this new coupling parameterization into the WAM model.

2.3.2 Numerical implementation

The numerical implementation of the new air-sea coupling module presented in the former section is concisely discussed here. It is based on a model presented by Elfouhaily *et al.* (1997), which is also adopted by Makin (1998). The calculation of the increment of the newly parameterized wind input source function $S_{\text{in}}^{\text{new}}$, from a certain time instant t_{old} to a time instant t_{new} at a specific location, requires growth rate γ^{new} at time t_{new}, which is calculated from equations (28)-(35). This requires the unknown wave spectrum F at t_{new} in (31) in order to determine the wave-induced stress. An approximation to $\gamma^{\text{new}}(t_{\text{new}})$ is calculated by solving the set of equations iteratively in the following way.

Firstly, it is noticed that the discrete frequency range of the prognostic part of the wave spectrum used in the WAM model is extended to calculate the new wind input source function in order to describe the high-frequency part of the spectrum more accurately. The discrete prognostic frequencies for which growth rate γ^{new} is calculated in the new wave model are given by $f_m = (1.1)^{m-1} f_1$, for $m = 1, 2, \ldots, 65$, ranging from $f_1 = 0.0418$ Hz to $f_{65} = 18.63$ Hz, instead of ranging from f_1 to $f_{25} = 0.4117$ Hz as implemented in the original WAM model. The original short discrete frequency range is still applied for the remaining source terms other than $S_{\text{in}}^{\text{new}}$. Calculation on this extended frequency grid is more time consuming, however.

One difficulty in determining the growth rate parameter is the fact that the wave-induced stress is dependent on the unknown wave spectrum, which is numerically solved as follows. The calculation of the wave-induced stress (30) requires F through omni-directional spectrum $\mathcal{T}$ of (31), in which saturation spectrum B was introduced,

$$F(k, \varphi) = k^{-4} B(k, \varphi). \tag{36}$$

This saturation spectrum B is written as a superposition of two spectra regimes similarly to the theory presented by Elfouhaily *et al.* (1997), i.e.

$$B(k, \varphi) = B_l(k, \varphi) + B_h(k) \Phi(k, \varphi), \tag{37}$$

where the long- and short-wave curvature spectra B_l and B_h and the angular spreading function Φ are defined as follows. In the current numerical implementation the long-wave curvature spectrum B_l accounting for the low-frequency part of the spectrum is defined by

$$B_l(k, \varphi) = k^4 F(k, \varphi) F_p, \tag{38}$$

which is approximated by using the wave spectrum F at the old time instant. The long-wave side-effect function F_p is given by

$$F_p = \exp\left\{-\frac{\Omega}{\sqrt{10}}\left(\sqrt{\frac{k}{k_p}}-1\right)\right\}, \tag{39}$$

in which $\Omega = U_{10}/c_p$ is the inverse wave age, $k_p = (2\pi f_p)^2/g$ is the wave number corresponding to the peak frequency f_p of the spectrum at the old time instant and c_p is its corresponding phase velocity.

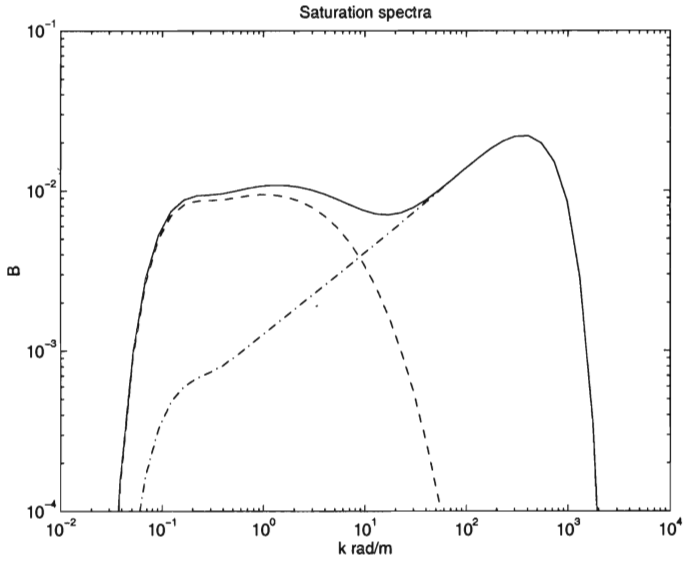

Figure 3: *Illustration of omni-directional spectrum B versus wave number k defined by superposition of long- and short-wave curvature spectra B_l and B_h.*

The parameterization of B_h is based on the empirical high-frequency spectrum designed for remote sensing applications by Elfouhaily *et al.* (1997) to describe the diagnostic tail accurately. It is defined by

$$B_h(k) = \frac{1}{2}\alpha_m \frac{c_m}{c} F_m J_p, \tag{40}$$

where $c_m = 0.23$ ms^{-1} is the phase speed at the secondary gravity-capillary peak and $\alpha_m = 0.0625u_*$ is the equilibrium range parameter for short waves. The short-wave side-effect function F_m and the JONSWAP peak enhancement function J_p are defined by

$$F_m = \exp\left\{-\frac{1}{4}\left(\frac{k}{k_m}-1\right)^2\right\}, \qquad J_p = (1.7+6\log\Omega)^{\Gamma}\exp\left\{-\frac{5}{4}\left(\frac{k_p}{k}\right)^2\right\}, \tag{41}$$

where $k_m = 363$ m^{-1}, $\Gamma = \exp\{-(\sqrt{k/k_p}-1)^2/2\sigma^2\}$ and $\sigma = 0.08\,(1+4\Omega^{-3})$. The angular spreading function Φ is used to seperate the uni-directional dependence of the wave spectrum from the angular spread,

$$2\pi\Phi = 1+\tanh\left(0.173+4\left(\frac{c}{c_p}\right)^{2.5}+0.565u_*\left(\frac{c_m}{c}\right)^{2.5}\right)\cos(2\varphi). \tag{42}$$

Figure 3 presents an illustration of a saturation spectrum B as a superposition of two spectra regimes defined according to (37). The effect of the energy cut-off caused by the side-effect functions F_p and F_m is apparent.

A numerical approximation of growth rate γ^{new} is found by iteratively solving equations (28)-(35) for a given wind input velocity U_{10} in order to calculate β of (33) at every discrete time step and at every location. Saturation spectrum B required for the wave-induced stress in (31) is approximated by expression (37) and it is kept constant during the iteration process. An analytic expression, dependent on k and k_p, is used as initial value of $\overline{f}$ of (34). A first approximation to u_* is obtained by a linear approximation of the relationship between $C_D = u_*^2/U_{10}^2$ and U_{10}, yielding also initial values for C_D and τ.

The initial values are used to start the iterations. First coupling parameter y and wave-induced stress τ_w are calculated. This produces a new value for $\overline{f}$ and a new drag coefficient C_D, yielding new values for the friction velocity u_* and the total stress τ. The new values are used as initial conditions for the next iteration, starting again by calculating the coupling parameter. In the current implementation two iteration steps are performed, in contrast to the numerical coupling module in WAM Cycle 4, which executes only one iteration step.

It is summarized that the numerical implementation of the air-sea interaction scheme uses an accurate approximation of the high-frequency tail, modelled on an extended frequency grid. The calculation of the numerical coupling parameter does not require a limiter in the new air-sea coupling scheme and the numerical implementation of the growth rate parameterization is consistent with the theory presented in the former section. A parameter tuning method is presented in the next section to balance the new wind input source function against the remaining source terms.

3 Parameter tuning method

This section describes a general method to estimate parameters occurring in the numerical wave model with respect to certain wave observations. It is used to tune the modified wind input source functions in the WAM model in the current studies. The iteration algorithm of the parameter tuning method is presented, which minimizes a cost-function, representing the model misfit of the wave parameters, by applying a finite difference approach together with the so-called Levenberg-Marquardt optimization method.

3.1 Cost-function

A certain set of parameters, the so-called control parameters, occur or are introduced in the source term equations of the WAM wave model. These control parameters, denoted by ψ_j, for $j = 1, 2, \ldots, M$, or,

$$\boldsymbol{\psi} = (\psi_1, \psi_2, \ldots, \psi_M)^T, \tag{43}$$

are to be tuned with regard to available wave observations. For this, several integral wave parameters, like H_s and f_p e.g., are used which are derived from the entire wave spectra calculated by the WAM model. The modelled integral wave parameters depend on the set of control parameters $\boldsymbol{\psi}$, location $\boldsymbol{x}$ and time t, and they are referred to by

$$\chi_i(\boldsymbol{\psi}; \boldsymbol{x}, t), \qquad i = 1, 2, \ldots, N. \tag{44}$$

The parameter tuning is performed by minimizing a cost-function expressing the misfit between the WAM model output of the integral wave parameters and their corresponding observations. Comparison of the calculated χ_i to their observations is performed for observation stations at locations $\boldsymbol{x} = x_n$, for $n = 1, 2, \ldots, S$, at discrete time instants $t = t_l$, for $l = 1, 2, \ldots, T_{i,n}$, where $T_{i,n}$ is the total number of time instants for which observed χ_i at station x_n is available and comparable to its corresponding WAM model output. The available observation of wave parameter χ_i at station x_n and at time instant t_l is denoted by $\chi_i^{\text{obs}}(x_n, t_l)$.

Cost-function J is defined for a certain set of control parameters $\boldsymbol{\psi}$ by the following superposition:

$$J(\boldsymbol{\psi}) = J^{\chi}(\boldsymbol{\psi}) + J^{\psi}(\boldsymbol{\psi}), \tag{45}$$

where functions J^{χ} and J^{ψ} are weighted sum of squares, see e.g. Holthuijsen *et al.* (1996) and Voorrips (1998), defined by

$$J^{\chi}(\boldsymbol{\psi}) = \sum_{i=1}^{N} \sum_{n=1}^{S} \sum_{l=1}^{T_{i,n}} \frac{1}{\sigma_{\chi_i}^2} \Big[\chi_i(\boldsymbol{\psi}; x_n, t_l) - \chi_i{}^{\text{obs}}(x_n, t_l) \Big]^2, \tag{46}$$

reflecting the statistics of errors in calculated and observed integral wave parameters, while

$$J^{\psi}(\boldsymbol{\psi}) = \sum_{j=1}^{M} \frac{1}{\sigma_{\psi_j}^2} \Big(\psi_j - \psi_j{}^{\text{fg}} \Big)^2, \tag{47}$$

represents the wave model confidence by expressing the deviation of the set of control parameters from a certain given first-guess set of control parameters $\boldsymbol{\psi}^{\text{fg}} = (\psi_1^{\text{fg}}, \psi_2^{\text{fg}}, \ldots, \psi_M^{\text{fg}})^T$. For the first-guess control parameters ψ_j^{fg}, $j = 1, 2, \ldots, M$ one can take e.g. the original control

parameter values occurring in the untuned WAM model. Weights σ_{χ_i} and σ_{ψ_j} are the given standard errors of χ_i and ψ_j, respectively, non-dimensionalizing cost-function J.

If $J(\boldsymbol{\psi}) < J(\boldsymbol{\psi}^{\mathrm{fg}})$ for a certain set $\boldsymbol{\psi}$ of control parameters, it follows that the modelled integral wave parameters χ_i obtained by the WAM model using $\boldsymbol{\psi}$ more accurately fit their observed values compared to those obtained by using the initial first-guess set $\boldsymbol{\psi}^{\mathrm{fg}}$. Minimizing cost-function J with respect to $\boldsymbol{\psi}$ provides an optimized set of tuned control parameters for which the WAM model produces more accurate wave parameter output. In other words, for a given first-guess set $\boldsymbol{\psi}^{\mathrm{fg}}$, a next set of control parameters $\boldsymbol{\psi}^{\mathrm{opt}} = (\psi_1^{\mathrm{opt}}, \psi_2^{\mathrm{opt}}, \ldots, \psi_M^{\mathrm{opt}})^T$ has to be constructed producing minimal cost, i.e. such that

$$J(\boldsymbol{\psi}^{\mathrm{opt}}) = \min_{\psi_1,\psi_2,\ldots,\psi_M} J(\boldsymbol{\psi}). \tag{48}$$

Calculating the minimum of non-linear function J is a difficult task which can not be done analytically in the studied situation. One way is to use the so-called adjoint wave model as described by Hersbach (1997, 1998). This method is not adopted here, however. The next section presents a numerical algorithm to produce approximations to $\boldsymbol{\psi}^{\mathrm{opt}}$ iteratively.

3.2 Levenberg-Marquardt optimization routine

The non-linear optimization method to minimize the cost-function used for the present studies is based on a finite difference approach together with the so-called Levenberg-Marquardt method. Its derivation describes one step of this iterative method, which is outlined, together with the numerical algorithm, in this section.

3.2.1 Derivation of the method

Minimization of the cost-function with respect to the set of control parameters requires the gradient of J to be zero. In other words, $\nabla J(\boldsymbol{\psi}^{\mathrm{opt}}) = \mathbf{0}$ at optimal value $\boldsymbol{\psi}^{\mathrm{opt}}$ of cost J, where ∇ denotes the gradient operator with respect to $\boldsymbol{\psi}$. So in order to find $\boldsymbol{\psi}^{\mathrm{opt}}$ from (48), the M equations

$$\frac{\partial J}{\partial \psi_j}(\boldsymbol{\psi}) = 0, \qquad j = 1, 2, \ldots, M \tag{49}$$

have to be solved with respect to $\boldsymbol{\psi}$. This set of equations is rewritten, after substitution of (45)-(47) into (49), by

$$\sum_{i=1}^{N} \sum_{n=1}^{S} \sum_{l=1}^{T_{i,n}} \frac{1}{\sigma_{\chi_i}^2} \Big[\chi_i(\boldsymbol{\psi}; x_n, t_l) - \chi_i{}^{\mathrm{obs}}(x_n, t_l)\Big] \frac{\partial \chi_i}{\partial \psi_j}(\boldsymbol{\psi}; x_n, t_l) + \\ + \frac{1}{\sigma_{\psi_j}^2} \Big(\psi_j - \psi_j{}^{\mathrm{fg}}\Big) = 0, \qquad j = 1, 2, \ldots, M. \tag{50}$$

Each wave parameter χ_i and gradient $\nabla\chi_i$ should be known functions of $\boldsymbol{\psi}$ in order to solve (50) with respect to $\boldsymbol{\psi}$. However, no explicit analytical expressions are available because wave parameters χ_i and their gradients depend on $\boldsymbol{\psi}$ in a complicated non-linear way through the WAM model. To overcome this problem, the following simplifying assumption is made, which is commonly applied in practice. It is assumed that the wave parameters can be well approximated by linear functions of $\boldsymbol{\psi}$ for each set of control parameters which is a small

perturbation of the given first-guess set of control parameters. In other words, each wave parameter χ_i is approximated for $\boldsymbol{\psi} \approx \boldsymbol{\psi}^{\mathrm{fg}}$ by its first-order Taylor-series expansion

$$\chi_i(\boldsymbol{\psi}) \approx \chi_i^{\mathrm{fg}} + \left(\boldsymbol{\psi} - \boldsymbol{\psi}^{\mathrm{fg}}\right)^T \cdot \nabla\chi_i(\boldsymbol{\psi}^{\mathrm{fg}}), \qquad i = 1, 2, \ldots, N, \tag{51}$$

which holds at every location x_n and time instant t_l. Here, $\chi_i^{\mathrm{fg}}(x_n, t_l) = \chi_i(\boldsymbol{\psi}^{\mathrm{fg}}; x_n, t_l)$ denotes the integral wave parameter using the first-guess set of control parameters for each x_n and t_l, obtained by performing one WAM model run.

Linearized expressions (51) show that the gradients of wave parameters χ_i are approximated by

$$\nabla\chi_i(\boldsymbol{\psi}) \approx \nabla\chi_i(\boldsymbol{\psi}^{\mathrm{fg}}), \qquad i = 1, 2, \ldots, N, \tag{52}$$

which are constant, but still unknown. However, they can be numerically approximated by their first-order differential quotients. For a given small perturbation $\boldsymbol{\varepsilon} = (\varepsilon_1, \varepsilon_2, \ldots, \varepsilon_M)^T$ of $\boldsymbol{\psi}^{\mathrm{fg}}$, the following finite difference approximation is applied to the gradients:

$$\frac{\partial\chi_i}{\partial\psi_j}(\boldsymbol{\psi}^{\mathrm{fg}}) \approx \frac{1}{\varepsilon_j}\left[\chi_i(\boldsymbol{\psi}^{\mathrm{fg}} + \varepsilon_j\mathbf{e}_j) - \chi_i^{\mathrm{fg}}\right], \tag{53}$$

defined for each wave and control parameter at every location and time instant, in which $\mathbf{e}_j = (0, \ldots, 0, 1, 0, \ldots, 0)^T$ is the j^{th} unit vector. Finite differential quotients (53) are calculated by making M additional WAM model runs using each perturbated set of control parameters $\boldsymbol{\psi}^{\mathrm{fg}} + \varepsilon_j\mathbf{e}_j$, for $j = 1, 2, \ldots, M$, which provide their corresponding wave parameters χ_i.

Substitution of (51)-(53) into (50) yields the following system of M linear equations for difference vector $\Delta\boldsymbol{\psi}$:

$$\mathbf{A} \cdot \Delta\boldsymbol{\psi} = \boldsymbol{b}, \qquad \Delta\boldsymbol{\psi} = \boldsymbol{\psi} - \boldsymbol{\psi}^{\mathrm{fg}}, \tag{54}$$

in which the components of square matrix $\mathbf{A}$ are given by

$$A_{j,k} = \begin{cases} \tilde{A}_{j,k} & (j \neq k) \\ \tilde{A}_{j,j} + \frac{1}{\sigma^2_{\psi_j}} & (j = k), \end{cases} \tag{55}$$

for $j, k = 1, 2, \ldots, M$, where coefficients $\tilde{A}_{j,k}$ are defined by

$$\tilde{A}_{j,k} = \sum_{i=1}^{N}\sum_{n=1}^{S}\sum_{l=1}^{T_{i,n}} \frac{1}{\sigma^2_{\chi_i}} d_{i,j}(x_n, t_l) d_{i,k}(x_n, t_l), \tag{56}$$

where the finite difference quotients of the wave parameters at x_n and t_l are denoted by

$$d_{i,j}(x_n, t_l) = \frac{1}{\varepsilon_j}\left[\chi_i(\boldsymbol{\psi}^{\mathrm{fg}} + \varepsilon_j\mathbf{e}_j; x_n, t_l) - \chi_i^{\mathrm{fg}}(x_n, t_l)\right], \tag{57}$$

for $i = 1, 2, \ldots, N$ and $j, k = 1, 2, \ldots, M$. The components of the right-hand side vector $\boldsymbol{b}$ are given by

$$b_j = \sum_{i=1}^{N}\sum_{n=1}^{S}\sum_{l=1}^{T_{i,n}} \frac{1}{\sigma^2_{\chi_i}}\left[\chi_i^{\mathrm{obs}}(x_n, t_l) - \chi_i^{\mathrm{fg}}(x_n, t_l)\right] d_{i,j}(x_n, t_l), \tag{58}$$

for $j = 1, 2, \ldots, M$. Solving linear system (54) with respect to $\Delta\boldsymbol{\psi}$ provides approximation $\boldsymbol{\psi}$ to the optimal tuned set of control parameters $\boldsymbol{\psi}^{\mathrm{opt}}$. It is noted that linear system (54) is equivalent to the one derived by Holthuijsen *et al.* (1996).

This approximation method to minimize cost-function J is also referred to as the optimization method of Newton because of the following. For $\boldsymbol{\psi} \approx \boldsymbol{\psi}^{\mathrm{fg}}$, the method of Newton approximates cost-function J by a second order Taylor-series and, besides that, assumes linearization (51) of the wave parameters. Differentiation of the quadratic cost-function yields a linear approximation to ∇J, whose zero is determined. It can be shown that the resulting linear system by this method is equal to (54).

The method of Newton constructs a new set $\boldsymbol{\psi}$ of control parameters from a given first-guess set $\boldsymbol{\psi}^{\mathrm{fg}}$ that should be a better approximation to $\boldsymbol{\psi}^{\mathrm{opt}}$ than $\boldsymbol{\psi}^{\mathrm{fg}}$ with respect to cost J. This method is efficient and accurately, provided assumption (51) is allowed, in other words, provided that $\boldsymbol{\psi}^{\mathrm{fg}}$ is sufficiently close to $\boldsymbol{\psi}^{\mathrm{opt}}$. However, it does not provide an accurate approximation $\boldsymbol{\psi}$ to $\boldsymbol{\psi}^{\mathrm{opt}}$ if the components of increment vector $\Delta\boldsymbol{\psi}$, found by solving (54), are too large. If cost J of $\boldsymbol{\psi}$, determined by solving (54), increases compared to the cost of $\boldsymbol{\psi}^{\mathrm{fg}}$, stepsize $\Delta\boldsymbol{\psi}$ should be reduced.

In the latter situation, it is efficient to use the so-called optimization method of steepest descent instead of the method of Newton, as proposed by e.g. Press *et al.* (1992). This method constructs, from a given first-guess set $\boldsymbol{\psi}^{\mathrm{fg}}$, approximation $\boldsymbol{\psi}$ to minimum $\boldsymbol{\psi}^{\mathrm{opt}}$ of cost J by taking a step down the gradient of J. In other words, each j^{th} component of increment vector $\Delta\boldsymbol{\psi}$ is defined by:

$$(\Delta\boldsymbol{\psi})_j = \psi_j - \psi_j^{\mathrm{fg}} = -\mu_j \frac{\partial J}{\partial \psi_j}(\boldsymbol{\psi}^{\mathrm{fg}}), \qquad j = 1, 2, \ldots, M, \tag{59}$$

where constants $\mu_j > 0$ are chosen small enough not to exhaust the downhill direction. In the current studies, special choice

$$\mu_j = \frac{1}{\lambda A_{j,j}}, \qquad j = 1, 2, \ldots, M, \tag{60}$$

as proposed by Press *et al.* (1992) and Marquardt (1963), is adopted, where $\lambda > 0$ is a user provided constant and components $A_{j,k}$ are defined in (55). Previous calculations show that right-hand side vector component b_j of (58) equals:

$$b_j = -\frac{\partial J}{\partial \psi_j}(\boldsymbol{\psi}^{\mathrm{fg}}), \qquad j = 1, 2, \ldots, M, \tag{61}$$

which yields, after substitution of (60)-(61) into (59), the following set of M uncoupled linear equations,

$$\lambda A_{j,j} (\Delta\boldsymbol{\psi})_j = b_j, \qquad j = 1, 2, \ldots, M. \tag{62}$$

Solving the set of M uncoupled linear equations (62), for an appropriate specified value of λ, provides approximation $\boldsymbol{\psi}$ to $\boldsymbol{\psi}^{\mathrm{opt}}$ which should be more accurate than $\boldsymbol{\psi}^{\mathrm{fg}}$ with respect to cost J. If this approximation still does not yield reduced cost compared to that of $\boldsymbol{\psi}^{\mathrm{fg}}$, one can narrow increment $\Delta\boldsymbol{\psi}$ by increasing value of λ and solve (62) again.

The method of Newton and the method of steepest descent are efficiently combined into one optimization method, the so-called method of Levenberg-Marquardt, which have been derived, independently, by Levenberg (1944) and Marquardt (1963), as descibed by Press *et al.* (1992). For cost-function (45), it combines the sets of equations (54) and (62) into one final resulting linear system, denoted by:

$$\hat{\mathbf{A}} \cdot \Delta\boldsymbol{\psi} = \boldsymbol{b}, \tag{63}$$

in which the components of square matrix $\hat{\mathbf{A}}$ are defined by

$$\hat{A}_{j,k} = \begin{cases} A_{j,k} & (j \neq k) \\ (1+\lambda)A_{j,j} & (j = k), \end{cases} \tag{64}$$

for $j, k = 1, 2, \ldots, M$, where components $A_{j,k}$ are defined in (55), vector $\boldsymbol{b}$ is defined in (58) and λ is a user specified constant. Solving linear system (63) with respect to $\Delta\boldsymbol{\psi}$ produces approximation $\boldsymbol{\psi}$ to the optimal tuned set of control parameters $\boldsymbol{\psi}^{\text{opt}}$, yielding reduced cost compared to that of $\boldsymbol{\psi}^{\text{fg}}$.

The method of Levenberg-Marquardt enables to vary between the method of Newton and the method of steepest descent by chosing parameter λ properly, depending on the cost of calculated approximation $\boldsymbol{\psi}$ compared to that of $\boldsymbol{\psi}^{\text{fg}}$. Matrix $\hat{A}$ from (64) is forced to be diagonally dominant for large λ, which reduces increment $\Delta\boldsymbol{\psi}$. In other words, linear system (63) approximately equals system (62), derived by the method of steepest descent, for large λ. On the other hand, for very small λ, system (63) reduces to (54) corresponding to the method of Newton. In practice one starts with small values of λ and increases λ if necessary.

The method of Levenberg-Marquardt allows a straightforward extension to an iterative routine, producing a sequence of control parameter vectors approximating $\boldsymbol{\psi}$ with increasing accuracy, as described in the next section.

3.2.2 Iterative optimization algorithm

The Levenberg-Marquardt optimization method (63) produces, starting from a given current set of control parameters, a new set of control parameters of decreased cost. This method can be extended to an iterative process creating a sequential set of approximations to $\boldsymbol{\psi}^{\text{opt}}$, each next approximation yielding lower cost than the preceding one. The algorithm of this iterative process, which is based on those presented by Marquardt (1963) and Press *et al.* (1992), is presented in Table 1 and it is described in the following.

Initially, a current set of control parameters $\boldsymbol{\psi}^{\text{cur}}$ is defined by the given first-guess set $\boldsymbol{\psi}^{\text{fg}}$. It takes $1 + M$ WAM model runs to determine wave parameters χ_i corresponding to $\boldsymbol{\psi}^{\text{cur}}$: 1 run using $\boldsymbol{\psi}^{\text{cur}}$ and M runs using its perturbations required to calculate gradients (57) of the wave parameters. The optimization routine starts with the method of Newton, in other words, it applies $\lambda = 0$ in the Levenberg-Marquardt method. Linear system (63) is solved, providing a next set of control parameters $\boldsymbol{\psi}^{\text{next}}$. One additional WAM model run using $\boldsymbol{\psi}^{\text{next}}$ is required to calculate cost J of $\boldsymbol{\psi}^{\text{next}}$.

The calculated set of control parameters $\boldsymbol{\psi}^{\text{next}}$ approximates $\boldsymbol{\psi}^{\text{opt}}$ more accurately than $\boldsymbol{\psi}^{\text{cur}}$, if cost $J(\boldsymbol{\psi}^{\text{next}}) < J(\boldsymbol{\psi}^{\text{cur}})$. In this case, the procedure is repeated by defining $\boldsymbol{\psi}^{\text{next}}$ as the new current set of control parameters. However, if cost $J(\boldsymbol{\psi}^{\text{next}}) > J(\boldsymbol{\psi}^{\text{cur}})$, constant λ has to be increased. Linear system (63) of Levenberg-Marquardt, now resembling the method of steepest descent, is solved yielding again a next set of control parameters $\boldsymbol{\psi}^{\text{next}}$. It is noted that no additional WAM model runs are required for this. One additional WAM model run is performed to calculate cost J of $\boldsymbol{\psi}^{\text{next}}$. If the cost of this $\boldsymbol{\psi}^{\text{next}}$ is less than that obtained by $\boldsymbol{\psi}^{\text{cur}}$, one starts again by defining $\boldsymbol{\psi}^{\text{next}}$ as the new current set of control parameters, using the Levenberg-Marquardt method resembling the method of Newton. If its cost is still not reduced enough, constant λ is increased and the Levenberg-Marquardt method resembling the method of steepest descent is applied again, and so on.

The iterative optimization algorithm is presented in Table 1. Notation $\mathbf{WAM}[\boldsymbol{\psi}]$ means 'perform a WAM model run using control parameters $\boldsymbol{\psi}$', and notation **LM** means 'solve

```
≫   λ := 0
≫   ψ^cur := ψ^fg
≫   WAM[ψ^cur] ⇒ J(ψ^cur)
≫   WAM[ψ^cur + ε_j e_j],  j = 1, 2, ..., M
≫   LM ⇒ ψ^next
≫   WAM[ψ^next] ⇒ J(ψ^next)
≫   stop := false

≫   repeat
≫     if J(ψ^next) ≤ J(ψ^cur) then
≫       if |J(ψ^next) − J(ψ^cur)| < ε then
≫         stop := true (⇒ ψ^opt := ψ^next)
≫       else
≫         decrease λ
≫         ψ^cur := ψ^next
≫         J(ψ^cur) := J(ψ^next)
≫         WAM[ψ^cur + ε_j e_j],  j = 1, 2, ..., M
≫         LM ⇒ ψ^next
≫         WAM[ψ^next] ⇒ J(ψ^next)
≫     else
≫       if λ < λ* then
≫         increase λ
≫         LM ⇒ ψ^next
≫         WAM[ψ^next] ⇒ J(ψ^next)
≫       else
≫         stop := true (⇒ ψ^opt := ψ^cur)
≫   until stop=true
```

Table 1: *Algorithm of the iterative parameter tuning method of Levenberg-Marquardt.*

the Levenberg-Marquardt set of equations (63)'. The iterative routine stops if no significant cost reduction is found for the calculated approximations of ψ^{opt}, which is represented by a certain small value of constant ϵ in the algorithm. It also stops if the method of steepest descent is not converging any further, which is displayed by a certain large constant λ^* in the algorithm. The iterative procedure of Levenberg-Marquardt described in Table 1 is applied for the parameter tuning in the current studies.

3.2.3 Further aspects

Various general aspects of the parameter tuning method with regard to the cost-function, the user provided parameters, and the implementation of the iterative algorithm are concisely remarked in this section.

Firstly, some remarks about the choice of cost-function J and its relation to constant λ occurring in the Levenberg-Marquardt method are outlined. In literature alternative for-

mulations of cost-function J exist, e.g cost $J = J^{\chi} + J^{\psi}$ of (45) is used by Holthuijsen *et al.* (1996) and Voorrips (1998), whereas cost-function $J = J^{\chi}$ defined by (46) is applied by Hersbach (1997, 1998) and Press *et al.* (1992). Applying the method of Newton to minimize cost-function $J = J^{\chi}$ analogously to the derivation described in Section 3.2.1, one obtaines the following linear system:

$$\tilde{\mathbf{A}} \cdot \Delta\boldsymbol{\psi} = \boldsymbol{b}, \tag{65}$$

in which the components of square matrix $\tilde{\mathbf{A}}$ are defined by (56). An iterative method together with its algorithm is described by Press *et al.* (1992) using cost-function $J = J^{\chi}$, which is based on the independent proposals of Levenberg (1944) and Marquardt (1963) and is therefore referred to as the Levenberg-Marquardt method. Both proposals are based on the required ability to adjust increment $\Delta\boldsymbol{\psi}$ calculated from (65) to ensure convergency. As proposed by Press *et al.* (1992), linear system (65) is therefore replaced by

$$\mathbf{A}^* \cdot \Delta\boldsymbol{\psi} = \boldsymbol{b}, \tag{66}$$

where the components of matrix $\mathbf{A}^*$ are defined by

$$A^*_{j,k} = \begin{cases} \tilde{A}_{j,k} & (j \neq k) \\ (1+\lambda)\tilde{A}_{j,j} & (j = k), \end{cases} \tag{67}$$

for $j, k = 1, 2, \ldots, M$, in which parameter λ adjusts increment $\Delta\boldsymbol{\psi}$ to ensure convergency. Alternative cost-function $J = J^{\chi} + J^{\psi}$ is used together with the optimization method of Newton by Holthuijsen *et al.* (1996), resulting in linear system (54). Compared to system (65), matrix components (55) show that additional cost-function J^{ψ} already yields a more diagonally dominant linear system producing a reduced increment $\Delta\boldsymbol{\psi}$. It is noted that only one iteration step of the method of Newton is performed in Holthuijsen *et al.* (1996), however. In the present study, cost-function $J = J^{\chi} + J^{\psi}$ is used and the Levenberg-Marquardt proposal is applied to (54), resulting in (63) containing constant λ to adjust increment $\Delta\boldsymbol{\psi}$. Therefore, optimization method (63) can be regarded as a generalization of the optimization methods described in Hersbach (1997, 1998), Holthuijsen *et al.* (1996) and Press *et al.* (1992).

The following can be said regarding the user provided constants. Initially, the Levenberg-Marquardt optimization method applies constant $\lambda = 0$, which is equivalent to the method of Newton. In case λ should be increased, equations (63) can be solved for various values of λ to check its dependence on $\boldsymbol{\psi}^{\text{next}}$. Initially increased constant $\lambda = 0.1$ is experienced to be a convenient value. Besides providing constant λ, the user is required to define perturbation vector $\boldsymbol{\varepsilon}$ to $\boldsymbol{\psi}^{\text{cur}}$ to calculate the differential quotients of the wave parameters. For this, values $\varepsilon_j = \psi_j^{\text{cur}}/10$ are experienced to be convenient. It is noted that, in each iteration step, a WAM model run is performed for each perturbated control parameter vector $\boldsymbol{\psi}^{\text{fg}} + \varepsilon_j \mathbf{e}_j$, for $j = 1, 2, \ldots, M$. Cost J of these M perturbated control parmeters can be calculated, which provides a useful insight into the behaviour of the cost-function.

One of the problems that generally arises using optimization routines is the difficulty of predicting the effect of the choice of initial control parameter set on the iteratively calculated approximations to the minimum. For example, the iterative method might diverge, converge to a local (in stead of the global) minimum, or even to a maximum. These problems can not be prevented at forehand because linearizations (51) and (53) are locally defined approximations. Trial and error using different initial control parameters sets gain insight into their effect, which is rather time consuming, however.

As already mentioned, each iteration step of the Levenberg-Marquardt optimization method requires, at least, $M + 1$ WAM model runs. For a large set of control parameters M this is rather time consuming, implying that only a limited number of iteration steps can be performed. Therefore, it is difficult to check the convergence in practice. Although only a limited number of control parameters is considered in the present studies, this inefficiency is a drawback of this numerical optimization method.

In the current studies, the iterative optimization method of Levenberg-Marquardt, which minimizes cost-function (45) by solving system (63) according to the algorithm of Table 1, is coded and implemented. It calculates, for a given initial set of control parameters and its corresponding WAM model data, a next approximation to the set of optimal control parameters and its cost. The iteration steps in the optimization algorithm are performed interactively by the user. The tuning method is adopted to estimate several control parameters introduced into the alternative wind input source terms of the WAM model as described in the next section.

4 Model results

The coupling parameterizations of WAM Cycel 4, the uncoupled air-sea interaction model and the newly developed air-sea coupling module presented in Section 2 are tuned according to wave observations at the North Sea by the iterative parameter estimation method outlined in the former section. Model results obtained by these alternative tuned coupling models are presented in this section. They are validated, intercompared and compared to those obtained by the original WAM Cycle 4 model. Firstly, the experimental set up is described and the wind input fields are analyzed.

4.1 Experimental set up

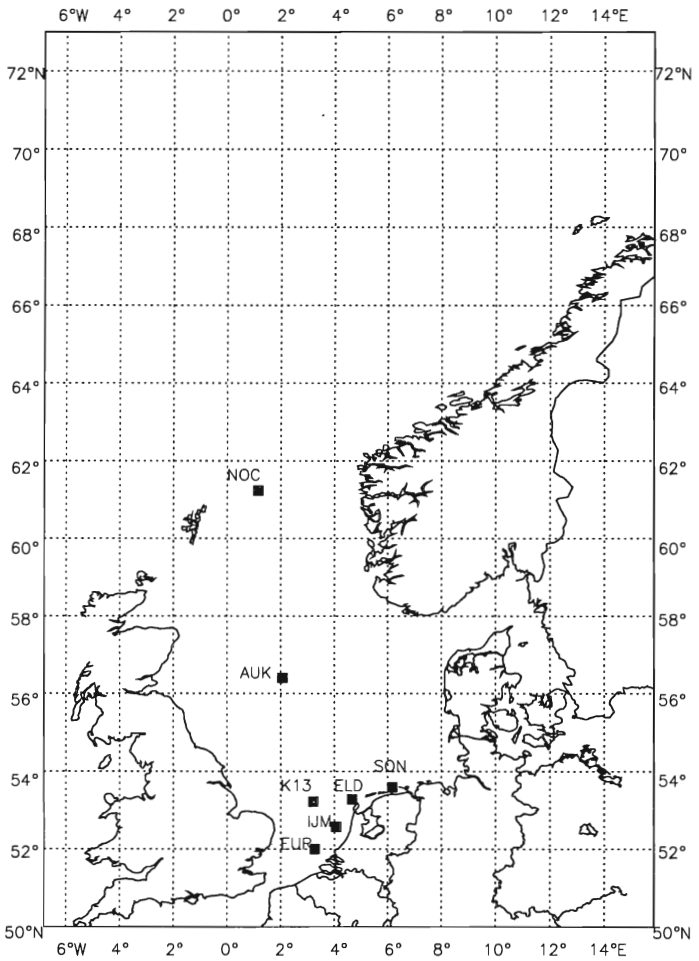

Figure 4: *Location of observation stations AUK, EURO, K13 and IJM in the North Sea.*

The numerical set up of the alternative WAM wave models, with or without modified source

terms, is identical to that of NEDWAM (NEDerlands WAve Model), which is a North Sea version of the global WAM model used operationally at KNMI. It takes into account the part of the North Sea running from 50.67°N to 70.00°N and from 7.50°W to 16.50°E as shown in Figure 4. This area is gridded by a spacing of 1/3 degree in latitudinal direction and 1/2 degree in longitudinal direction. The wave directions are discretized into 12 bins, and the frequency grid contains 25 frequencies from 0.0418 up to 0.4117 Hz arranged according to a logarithmic scale. The model propagation and source term integration time step is 600 s. The model is driven by the given 10 meter wind velocities with a wind time step of 3 hours. The WAM model output of the performed hindcast runs is archived every 3 hours. For further details, see Burgers (1990) and Günther *et al.* (1992).

Parameters occuring in the source functions (2) are tuned to balance the modified wind input source term to the remaining source functions occurring in the WAM model. This parameter tuning is performed for the (tuning) time period 1-30 December, 1998. Stormy weather occurred on the North Sea at the beginning and the end of December accompanied by hard winds, $U_{10} \sim 20$ ms^{-1}, and large ocean waves $H_s \sim 4.5$ m, while more quiet weather, $U_{10} \sim 8$ ms^{-1} and $H_s \sim 2$ m, occurred in the middle of December. The combination of quiet and stormy weather is necessary to create tuned parameters which are representative to all kinds of weather.

Cost-function (45) is based on the error between the modelled and the observed values of the integral wave parameters mean wave height (15) and peak frequency (16),

$$\chi_1 = H_s, \qquad \chi_2 = f_p, \tag{68}$$

together with their previously determined standard errrors $\sigma_{H_s} = 0.5$ m and $\sigma_{f_p} = 1.0$ Hz. The misfit of these wave parameters is minimized at four observation stations AUK (56.4°N, 2.1°E), EURO (52.0°N, 3.3°E), K13 (53.2°N, 3.2°E) and IJM (52.6°N, 4.1°E), which are Wavec buoys located near (oil-)platforms producing three-hourly wave observations. Figure 4 indicates their locations. Reliable and fairly complete wave observation sets were available for these stations. Although station NOC is located at the interesting northern part of the North Sea, its observations are not applied in the current model tuning and validation studies because they consist of rather low quality and incomplete data sets for the time periods taken into consideration.

The modified and tuned WAM models are validated and mutually compared for two different (validation) time periods, November 1 - December 21, 1997 and 1-24 January, 1998. Stormy weather as well as quiet weather occurred during both validation time periods. Statistical quantities are used to compare the output of the different models to each other and to the observations. The bias, standard deviation and root-mean-square of the error between the modelled and observed values of a wave- or wind parameter ζ, for each observation station x_n, $n = 1, \ldots, 4$, are defined, respectively, by:

$$Bias(\zeta, x_n) = \frac{1}{T_n} \sum_{l=1}^{T_n} \left[\zeta(x_n, t_l) - \zeta^{\text{obs}}(x_n, t_l) \right], \tag{69}$$

$$SD(\zeta, x_n)^2 = \frac{1}{T_n} \sum_{l=1}^{T_n} \left[\zeta(x_n, t_l) - \zeta^{\text{obs}}(x_n, t_l) - Bias(\zeta, x_n) \right]^2, \tag{70}$$

$$RMS(\zeta, x_n)^2 = \frac{1}{T_n} \sum_{l=1}^{T_n} \left[\zeta(x_n, t_l) - \zeta^{\text{obs}}(x_n, t_l) \right]^2, \tag{71}$$

where ζ^{obs} is the observation of the wave- or wind parameter ζ and T_n is the number of time instants for which observations ζ^{obs} are available at station x_n. The bias represents the deviation of the mean modelled value of parameter ζ from its mean observed value, while the standard deviation reflects the mean fluctuation of the modelled error of ζ around its mean. Note that a positive (negative) bias implies a mean over- (under-) approximation of ζ compared to the observations. The root-mean-square is related to the bias and the standard deviation by the Pythagorean theorem,

$$RMS^2 = Bias^2 + SD^2. \tag{72}$$

The number of available observations T_n of significant wave height H_s^{obs} and peak frequency f_p^{obs} at station x_n is given in Tables 2 and 4 for each time period. The statistical quantities are used for WAM model verification and for wind input analysis, as described in the next section.

4.2 Wind input analysis

The input of the WAM model consists of wind velocity fields at 10 m height, which are required every 3 hours. The atmospheric model HIRLAM (HIgh Resolution Limited Area Model), which is used operationally at KNMI, provides these wind fields for each time period of the hindcast WAM model runs. The wind velocity fields at 10 m height, which are previously calculated by HIRLAM and interpolated to the WAM grid, are denoted by U_{10}.

The quality of the modelled wind input fields U_{10} is analyzed by their comparison to the observed wind velocity fields. Wind velocities are not measured at the required 10 m height at the considered observation stations, e.g. the wind sensor at oil-platforms AUK and K13 is mounted on top of a high derrick, reaching 103.3 m and 73.8 m, respectively. Therefore, the observed wind velocities are corrected to 10 m height according to Benschop (1996), which are referred to as U_{10}^{obs}.

Statistical quantities (69)-(71) are calculated for the modelled wind input parameter $\zeta = U_{10}$ for each station and each time period. The relative errors are studied by using the mean modelled and mean observed 10 m wind velocities for each station x_n, $n = 1, \ldots, 4$, defined by:

$$\overline{U}_{10}(x_n) = \frac{1}{T_{\text{mod}}} \sum_{l=1}^{T_{\text{mod}}} U_{10}(x_n, t_l), \qquad \overline{U_{10}^{\text{obs}}}(x_n) = \frac{1}{T_n} \sum_{l=1}^{T_n} U_{10}^{\text{obs}}(x_n, t_l), \tag{73}$$

where T_{mod} is the number of time instants for which U_{10} is calculated by the HIRLAM model, equalling $T_{\text{mod}} = 240$ for tuning time period Dec '98, and $T_{\text{mod}} = 408$ and 192 for validation time periods Nov/Dec '97 and Jan '98, respectively. The number of observations T_n of wind velocity U_{10}^{obs} at station x_n is given in Tables 2 and 4 and the calculated statistics are presented in Tables 3 and 5. The complete time series of the modelled U_{10} together with their observations are displayed in Figures 11-13 of Appendix A.1 for each time period.

The statistics and time series show that the wind velocities during time period Dec' 98 are accurately modelled by HIRLAM. Around 30% of the wind observation data is lacking at AUK and IJM. The high winds at AUK are over-estimated by the model, while the lower winds at the remaining stations are under-estimated during this time period.

For both time periods Nov/Dec '97 and Jan '98, the observations show rather low wind velocities at station AUK compared to the observed winds at the other stations, which is usually not the case. The modelled U_{10} show a high bias at station AUK, and only $60 - 80\%$

T_n (# obs)	Dec '98 AUK	EURO	K13	IJM
U_{10}^{obs}	166	240	239	159
$H_s^{\text{obs}}, f_p^{\text{obs}}$	226	240	239	168

Table 2: *Number of observations T_n of wind velocity U_{10}, significant wave height H_s and peak frequency f_p at each observation station x_n for tuning time period Dec '98.*

U_{10} [m/s]	Dec '98 AUK	EURO	K13	IJM
BIAS	0.40	−0.82	−0.41	−0.28
SD	1.29	1.51	1.33	1.63
RMS	1.36	1.72	1.39	1.65
$\overline{U}_{10}$	10.11	8.59	8.99	8.98
$\overline{U_{10}^{\text{obs}}}$	9.65	9.42	9.36	9.52

Table 3: *Statistics of errors between modelled and observed wind input U_{10}, and mean values of modelled and observed U_{10} at each observation station for tuning time period Dec '98.*

T_n (# obs)	Nov/Dec '97 AUK	EURO	K13	IJM	Jan '98 AUK	EURO	K13	IJM
U_{10}^{obs}	330	383	367	379	117	192	189	189
$H_s^{\text{obs}}, f_p^{\text{obs}}$	332	388	367	408	118	192	189	191

Table 4: *Number of observations T_n of wind velocity U_{10}, significant wave height H_s and peak frequency f_p at each observation station x_n for validation time periods Nov/Dec '97 and Jan '98.*

U_{10} [m/s]	Nov/Dec '97				Jan '98			
	AUK	EURO	K13	IJM	AUK	EURO	K13	IJM
BIAS	1.93	−1.09	−0.20	0.09	2.54	−1.17	−0.71	0.28
SD	1.63	1.35	1.21	1.63	2.30	1.11	1.46	1.51
RMS	2.53	1.73	1.22	1.64	3.43	1.61	1.63	1.54
$\overline{U}_{10}$	9.82	7.91	8.64	8.46	9.82	10.48	10.62	10.80
$\overline{U}_{10}^{\text{obs}}$	7.81	9.08	8.86	8.37	7.50	11.66	11.31	10.49

Table 5: *Statistics of errors between modelled and observed wind input U_{10}, and mean values of modelled and observed U_{10} at each observation station for validation time periods Nov/Dec '97 and Jan '98.*

of the observations at AUK are available for these periods. Nevertheless, the observations of U_{10} at station AUK are taken into account for the model experiments because of its important northern location at the modelled area of the North Sea. The modelled winds at AUK and IJM are over-estimated, while they are under-estimated at EURO and K13.

Because the wave height is coupled to the wind input, it is expected that the WAM model produces over- (under-) approximations of the wave heights at those stations for which over- (under-) estimations to the wind input velocity are supplied. This consistency is assessed for the various air-sea coupling models in Section 4.4.

4.3 Parameter tuning

The alternative parameterizations of the wind input source term described by the WAM Cycle 4 model, the uncoupled air-sea model and the new air-sea coupling routine are balanced against the remaining source functions in the WAM model. One or two control parameters are introduced in each wave model, which are tuned against wave observations by applying the iterative optimization method of Levenberg-Marquardt presented in Section 3.2.2. This is done for tuning time period Dec '98 using the experimental set up for the North Sea described in Section 4.1.

4.3.1 One control parameter

Firstly, one control parameter is considered in the wave models. The Charnock constant is tuned in the uncoupled air-sea model, and the overall strength of the dissipation source term is tuned in the new air-sea coupling module and the WAM Cycle 4 model.

Uncoupled air-sea scheme. The modified wind input source term in the WAM model that does not incorporate the coupling back of the sea state to the wind velocity profile was presented in Section 2.2. It assumes a zero coupling parameter, implying a constant Charnock parameter $\alpha = \hat{\alpha}$ through (6) and (8), resulting in relation (26). The Charnock constant is

the only control parameter which is tuned in this uncoupled air-sea parameterization, i.e.

$$\psi_1 = \alpha = \hat{\alpha} = \frac{z_0 g}{u_*^2}. \tag{74}$$

The first-guess control parameter is defined by $\alpha^{\mathrm{fg}} = 0.025$ and the standard error is given by $\sigma_\alpha = 0.0125$.

The iterative parameter optimization method is executed to tune the Charnock control parameter with regard to observations of H_s and f_p at the four observation stations during time period Dec '98. It took 2 iteration steps of the Levenberg-Marquardt method and 5 WAM model runs in total to find the optimal value of α yielding minimal cost. The cost of the current control parameter and its perturbated value required for the gradient of the cost-function is calculated in each iteration step. Several additional WAM model runs have been performed to display the global behaviour of the cost-function. Figure 5 shows an approximate representation of cost J as a function of α found by interpolation.

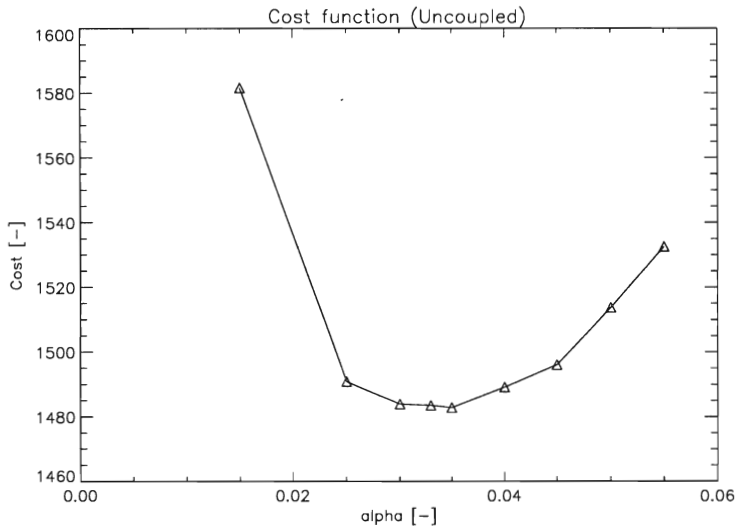

Figure 5: *Cost-function J of control parameter $\psi = \alpha$ representing Charnock constant $\hat{\alpha} = z_0 g / u_*^2$ in the uncoupled air-sea wave model.*

The calculated optimized Charnock constant α^{opt} in the uncoupled air-sea interaction parameterization reads

$$\alpha^{\mathrm{opt}} = 0.035, \tag{75}$$

as can also be seen from Figure 5. The tuned Charnock parameter produces minimal cost $J(0.035) = 1483$, whereas the original WAM Cycle 4 model yields cost $J = 1344$ for the same time period Dec '98. An additional WAM model run of the uncoupled model using α^{opt} is performed for each validation time period Nov/Dec '97 and Jan '98 yielding cost $J(0.035) = 3221$ and 1211, respectively, whereas costs $J = 3080$ and 1139 are produced by the original WAM Cycle 4 model. The cost of the tuned uncoupled model is slightly higher for each time period compared to the cost obtained by the original WAM Cycle 4 model, but it is still of the same order. Table 6 displays the calculated cost values.

Note that the tuned uncoupled air-sea model using optimized Charnock constant (75) is equivalent to the original WAM Cycle 4 model applied with a constant coupling parameter

$y = 0.92$ instead of dynamic air-sea coupling relation (8). The tuned uncoupled air-sea model is validated and compared to the other air-sea parameterizations in Section 4.4.

New air-sea coupling module. The description of the new air-sea coupling model is presented in Section 2.3. The wind input source function of the original WAM model is replaced by a new parameterization. This new wind input source term is balanced against the white-capping dissipation source term S_{dis} of (12). A dimensionless control parameter ψ_{dis} is introduced into the modified wave model by replacing overall strength C_{dis} of the dissipation source term S_{dis} of (12) by

$$C_{\text{dis}} \rightarrow \psi_{\text{dis}} C_{\text{dis}}, \tag{76}$$

where constant $C_{\text{dis}} = 9.4 \times 10^{-5}$ is the value occurring in the original WAM Cycle 4 model. The only control parameter which is tuned is $\psi_1 = \psi_{\text{dis}}$. The first-guess control parameter is defined by $\psi_{\text{dis}}^{\text{fg}} = 0.50$ and the standard error is given by $\sigma_{\psi_{\text{dis}}} = 0.05$.

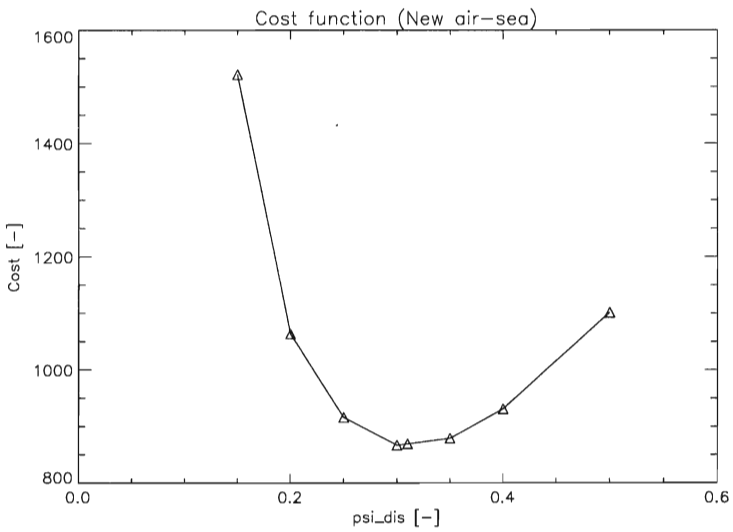

Figure 6: *Cost-function J of control parameter ψ_{dis} representing the overall strength of the dissipation source term in the modified WAM model containing the new air-sea coupling parameterization.*

The optimal value of ψ_{dis} producing minimal cost for tuning period of Dec '98 is obtained by performing 3 iterations of the Levenberg-Marquardt parameter optimization method and 6 WAM model runs. Figure 6 displays the interpolated cost-function of ψ_{dis}, found during the iteration process together with several additional WAM model runs.

Figure 6 shows that the parameter optimization method yields the optimal control parameter $\psi_{\text{dis}}^{\text{opt}}$, together with the corresponding tuned overall strength $C_{\text{dis}}^{\text{opt}}$ of the dissipation source term,

$$\psi_{\text{dis}}^{\text{opt}} = 0.30, \qquad C_{\text{dis}}^{\text{opt}} = 2.82 \times 10^{-5}, \tag{77}$$

producing minimal cost $J(0.30) = 867$, whereas the original WAM Cycle 4 model produces cost $J = 1344$. An additional WAM model run of the new air-sea coupling scheme using $\psi_{\text{dis}}^{\text{opt}}$ is performed for both validation time periods Nov/Dec '97 and Jan '98 yielding cost $J(0.30) = 1699$ and 658, respectively, while $J = 3080$ and 1139 are obtained by the original WAM Cycle 4 model. Table 6 displays the calculated cost values. The modified WAM

model containing the new wind input source term together with the 70%-reduced dissipation source term produces a considerably reduced cost compared to the original WAM Cycle 4 wave model for each time period. It is noted however, that this comparison is not completely fair because the overall strength of the dissipation source term in the original WAM model has not been tuned to this wave observation data set, this will be done in the following. The tuned new air-sea coupling parameterization is validated and compared to the other air-sea coupling models in Section 4.4.

Original WAM Cycle 4 model. Also the original WAM Cycle 4 model, described in Section 2.1, is tuned with respect to the overall strength C_{dis} of the dissipation source term in order to make an honest comparison to the tuned new air-sea interaction module.

Control parameter $\psi_1 = \psi_{\text{dis}}$ of (76) is introduced into the dissipation source term S_{dis} of the original WAM model, where $C_{\text{dis}} = 9.4 \times 10^{-5}$, $\psi_{\text{dis}}^{\text{fg}} = 1.0$ and $\sigma_{\psi_{\text{dis}}} = 0.05$.

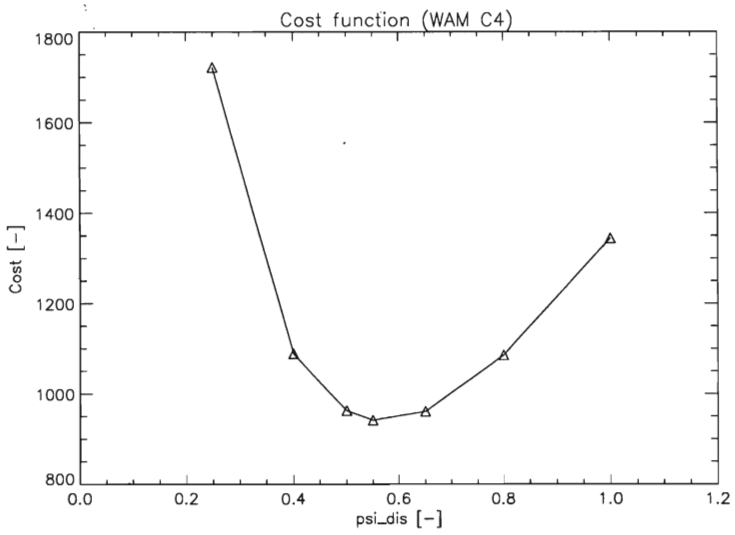

Figure 7: *Cost-function J of control parameter ψ_{dis} representing the overall strength of the dissipation source term in the original WAM Cycle 4 model.*

The optimal value of ψ_{dis} producing minimal cost for the tuning period of Dec '98 is obtained by performing 2 iterations of the Levenberg-Marquardt parameter optimization method and 5 WAM model runs. Figure 7 displays the interpolated cost-function of ψ_{dis}, found during the iteration process together with several additional WAM model runs.

Figure 7 shows that the parameter optimization method yields the optimal control parameter $\psi_{\text{dis}}^{\text{opt}}$, together with the corresponding tuned overall strength $C_{\text{dis}}^{\text{opt}}$ of the dissipation source term,

$$\psi_{\text{dis}}^{\text{opt}} = 0.55, \qquad C_{\text{dis}}^{\text{opt}} = 5.17 \times 10^{-5}, \tag{78}$$

producing minimal cost $J(0.55) = 942$, whereas the original WAM Cycle 4 model produces cost $J = 1344$. An additional run of the tuned WAM Cycle 4 model using $\psi_{\text{dis}}^{\text{opt}}$ is performed for both validation time periods Nov/Dec '97 and Jan '98 yielding cost $J(0.55) = 2019$ and 655, respectively, while $J = 3080$ and 1139 are obtained by the original WAM Cycle 4 model.

Table 6 displays the calculated cost values. It shows that the tuned WAM Cycle 4 model containing the 45%-reduced dissipation source term produces a considerably decreased cost

compared to the original WAM Cycle 4 wave model for each time period. Compared to the tuned new air-sea parameterization (77), it produces a higher cost for tuning time period Dec '98 and validation time period Nov/Dec '97 and a slightly lower cost for validation time period Jan '98, although they are still of the same order. The tuned WAM Cycle 4 model is validated and compared to the other air-sea coupling models in Section 4.4.

4.3.2 Two control parameters

Both the Charnock constant and the overall strength of the dissipation source term are tuned in the uncoupled air-sea model and the original WAM Cycle 4 model in order to intercompare the three alternative air-sea interaction schemes.

Uncoupled air-sea coupling scheme. Two control parameters are tuned in the WAM model that incorporates the uncoupled air-sea parameterization described in Section 2.2. These parameters are the Charnock constant $\hat{\alpha} = \alpha$ of (74) and the overall strength of the dissipation source term $\psi_{\rm dis}$ introduced in (76). This means that cost-function J of the 2-dimensional control parameter vector

$$\boldsymbol{\psi} = (\psi_1, \psi_2)^T = (\hat{\alpha}, \psi_{\rm dis})^T \tag{79}$$

is minimized with respect to both components. The first-guess control parameter is defined by $\boldsymbol{\psi}^{\rm fg} = (\alpha^{\rm fg}, \psi_{\rm dis}^{\rm fg})^T = (0.01, 1.0)^T$. The optimal control parameter vector $\boldsymbol{\psi}^{\rm opt}$ producing minimal cost is obtained by performing 3 iterations of the Levenberg-Marquardt method and 10 WAM model runs. Several additional model runs are performed to examine the global behaviour of the cost-function. The calculated components of $\boldsymbol{\psi}^{\rm opt}$ are given by

$$\alpha^{\rm opt} = 0.0125, \qquad \psi_{\rm dis}^{\rm opt} = 0.40, \tag{80}$$

together with $C_{\rm dis}^{\rm opt} = 3.76 \times 10^{-5}$. The cost of optimized control parameter vector (80) reads $J(0.0125, 0.40) = 897$ for tuning time period Dec '98, while $J(0.0125, 0.40) = 1837$ and 668 are found for validation time periods Nov/Dec '97 and Jan '98, respectively.

The results in Table 6 show that the tuned uncoupled air-sea model using parameters (80) produces considerably reduced cost compared to the original WAM model and the uncoupled air-sea scheme using tuned Charnock constant (75) only. It produces a slightly higher cost compared to the new air-sea module using tuned dissipation (77) only, although they are still of the same order. The tuned uncoupled model is validated and compared to the other air-sea coupling models in Section 4.4.

Original WAM Cycle 4. Two control parameters are tuned in the original WAM model in order to make an honest comparison between the two alternative air-sea coupling modules. These parameters are constant $\hat{\alpha}$ defined in relation (8) and the overall strength of the dissipation source term $\psi_{\rm dis}$ introduced in (76). This means that cost-function J of the 2-dimensional control parameter vector $\boldsymbol{\psi}$ of (79) is minimized with respect to both components. The first-guess control parameter is defined by $\boldsymbol{\psi}^{\rm fg} = (\hat{\alpha}^{\rm fg}, \psi_{\rm dis}^{\rm fg})^T = (0.01, 1.0)^T$. The optimal control parameter vector $\boldsymbol{\psi}^{\rm opt}$ producing minimal cost is obtained by performing 4 iterations of the Levenberg-Marquardt method and 14 WAM model runs. Several additional model runs are performed to examine the global behaviour of the cost-function. The calculated components of the optimal control parameter vector $\boldsymbol{\psi}^{\rm opt}$ are given by

$$\hat{\alpha}^{\rm opt} = 0.0060, \qquad \psi_{\rm dis}^{\rm opt} = 0.57, \tag{81}$$

Cost J [-]			Tuning Dec '98	Validation Nov/Dec '97	Jan '98
	$\hat{\alpha}$	ψ_{dis}			
WAM C4	0.010	1.00	1344	3080	1139
Uncoupled	0.035	1.00	1483	3221	1211
New air-sea	–	0.30	867	1699	658
WAM C4	0.010	0.55	942	2019	655
Uncoupled	0.0125	0.40	897	1837	668
WAM C4	0.0060	0.57	909	1983	645
Regression	0.010	1.00	1433	3115	1193

Table 6: *Cost J of control parameter $\psi = (\hat{\alpha}, \psi_{\text{dis}})^T$ obtained by the various (tuned) air-sea coupling modules described in Sections 4.3.1, 4.3.2 and 4.4.1 for each time period ($\hat{\alpha} = 0.010$ and $\psi_{\text{dis}} = 1.00$ are the original untuned values).*

yielding $C_{\text{dis}}^{\text{opt}} = 5.36 \times 10^{-5}$. The cost of the optimized control parameter vector (81) reads $J(0.006, 0.57) = 909$ for tuning time period Dec '98, while $J(0.006, 0.57) = 1983$ and 645 are found for validation time periods Nov/Dec '97 and Jan '98, respectively.

The results in Table 6 show that the tuned WAM Cycle 4 model using parameters (81) produces considerably reduced cost compared to the original WAM model and the uncoupled air-sea scheme using tuned Charnock constant (75) only. Compared to the WAM Cycle 4 model that is tuned to the dissipation only, it produces a reduced cost, although they are still of the same order. It produces a slightly higher cost compared to the new air-sea module using only tuned dissipation (77) for Dec '98 and Nov/Dec '97, while it produces lower cost for Jan '98, although they are still of the same order. The same holds for the uncoupled air-sea module that is tuned for both control parameters as can be seen in Table 6. The tuned WAM Cycle 4 model is validated and compared to the other air-sea coupling models in Section 4.4.

4.4 Validation and comparison of air-sea coupling modules

The performances of the (tuned) WAM Cycle 4 model, the tuned uncoupled air-sea scheme and the tuned new air-sea interaction parameterization are assessed in this section. These coupling modules are verified and validated by comparing the wave model output to each other and to the wave observations, which is done by studying statistics, time series and scatter plots of various wave parameters.

4.4.1 Statistics and time series of tuning wave parameters

The calculated costs displayed in Table 6 show that the original WAM Cycle 4 model and the tuned uncoupled air-sea scheme ($\alpha = 0.035$) are expected to produce approximately equally accurate results for H_s and f_p. The same holds for the remaining four tuned air-sea parameterizations. It is noted that the original WAM Cycle 4 model produces under-estimations of H_s and f_p, which is reflected by the negative biases of their modelling errors. The time series show that H_s is principally under-estimated for large waves during stormy

periods where $U_{10} > 15$ ms^{-1}.

Firstly, the following is said concerning the numerical coupling parameter in the WAM Cycle 4 model. Figure 2 in Section 2.1.2 presents regression curve y^{reg} of (21), describing an explicit relationship for the numerical coupling parameter in the WAM model. This regression curve is implemented into the WAM Cycle 4 model, replacing the original numerical coupling parameterization (18). A WAM model run is executed for each time period and the corresponding cost-function is calculated. The results are shown on the last row of Table 6. It shows that the cost obtained by applying the implemented regression curve is only little higher compared to the original WAM Cycle 4 model for each time period. Also the statistics of the modelling errors of H_s and f_p are calculated, they are displayed on the last rows of Tables 7-10. Comparing them to the statistics obtained by the original WAM Cycle 4 model, it is found that both models produce equally accurate values of H_s and f_p at each station for each time period. The time series of H_s, which are not displayed here, show that the original WAM Cycle 4 model produces wave heights which are at a few time instants approximately only 10 cm larger. This holds except for one exceptional time instant at station AUK in Dec '98 where $H_s > 11$ m, here the original model produces an almost 1 m lower H_s than the model using the regression curve. One may conclude that numerical coupling parameter y in the original coupling scheme in the WAM Cycle 4 model can be replaced by regression curve (21) without losing the accuracy of the calculated H_s and f_p.

The performance of the (tuned) WAM Cycle 4 model, the tuned uncoupled air-sea model and the tuned new air-sea coupling module presented in the former section are studied by considering the bias, standard deviation and root-mean-square of the modelling errors of wave parameters $\zeta = H_s$ and f_p defined in (68)-(70). For tuning the modified wave models, these wave parameters were taken into account by minimizing the misfit between their calculated and observed values for time period Dec '98. The results of the calculated statistics are presented in Tables 7 and 9. The tuned modified wave models are validated for time periods Nov/Dec '97 and Jan '98. Again, the statistics of modelling errors of H_s and f_p obtained by the alternative coupling schemes are calculated, and the results are presented in Tables 8 and 10. The complete time series of significant wave height H_s calculated by the original WAM Cycle 4 model, the tuned uncoupled model (75), the tuned new air-sea coupling module (77) and the tuned WAM Cycle 4 model (78) together with observations H_s^{obs} are presented in Figures 14-16 of Appendix A.2. The time series and statistics are used to validate and intercompare these air-sea coupling modules.

From the statistics and the time series it can be concluded that the performances of the original WAM Cycle 4 model and the tuned uncoupled air-sea model ($\alpha = 0.035$) are approximately equally accurate with respect to H_s and f_p for each time period, the original coupled module performs just slightly better. The influence of the dynamic air-sea coupling applied in the original WAM Cycle 4 model on the calculated significant wave height is rather small compared to the uncoupled parameterization. The remaining four tuned coupling modules show a reduction of the root-mean-square of the modelling errors of H_s and f_p for each time period. It is clear that the standard deviation is not affected much by the parameter tuning, which means that the decreased root-mean-square for the tuned new coupling module is caused by a reduced bias through (72).

Comparison of the results obtained by the original WAM Cycle 4 model to those obtained by the tuned new air-sea module ($\psi_{\text{dis}} = 0.30$) and the tuned WAM Cycle 4 model ($\psi_{\text{dis}} = 0.55$) leads to the conclusion that both tuned schemes perform significantly better than the

H_s [m]			Dec '98			
			AUK	EURO	K13	IJM
	$\hat{\alpha}$	ψ_{dis}		*BIAS*		
WAM C4	0.010	1.00	−0.42	−0.33	−0.36	−0.25
Uncoupled	0.035	1.00	−0.44	−0.36	−0.39	−0.27
New air-sea	–	0.30	0.10	−0.04	0.02	0.07
WAM C4	0.010	0.55	−0.01	−0.14	−0.10	0.00
Uncoupled	0.0125	0.40	0.03	−0.12	−0.06	0.00
WAM C4	0.0060	0.57	−0.03	−0.14	−0.10	0.00
Regression	0.010	1.00	−0.45	−0.35	−0.38	−0.28
	$\hat{\alpha}$	ψ_{dis}		*SD*		
WAM C4	0.010	1.00	0.41	0.27	0.34	0.28
Uncoupled	0.035	1.00	0.42	0.27	0.34	0.28
New air-sea	–	0.30	0.44	0.27	0.33	0.30
WAM C4	0.010	0.55	0.45	0.27	0.33	0.32
Uncoupled	0.0125	0.40	0.44	0.26	0.33	0.30
WAM C4	0.0060	0.57	0.46	0.26	0.32	0.32
Regression	0.010	1.00	0.43	0.27	0.34	0.28
	$\hat{\alpha}$	ψ_{dis}		*RMS*		
WAM C4	0.010	1.00	0.58	0.43	0.49	0.38
Uncoupled	0.035	1.00	0.61	0.45	0.51	0.39
New air-sea	–	0.30	0.45	0.27	0.33	0.31
WAM C4	0.010	0.55	0.45	0.30	0.34	0.32
Uncoupled	0.0125	0.40	0.44	0.29	0.33	0.30
WAM C4	0.0060	0.57	0.46	0.30	0.34	0.32
Regression	0.010	1.00	0.62	0.44	0.51	0.39

Table 7: *Bias, standard deviation and root-mean-square of the modelling error of H_s obtained by the (tuned) WAM Cycle 4 model, the tuned uncoupled air-sea model and the tuned new air-sea coupling module at each station for tuning time period Dec '98.*

H_s [m]			Nov/Dec '97				Jan '98			
			AUK	EURO	K13	IJM	AUK	EURO	K13	IJM
	$\hat{\alpha}$	ψ_{dis}	*BIAS*				*BIAS*			
WAM C4	0.010	1.00	−0.49	−0.32	−0.47	−0.20	−0.38	−0.39	−0.44	−0.25
Uncoupled	0.035	1.00	−0.50	−0.35	−0.49	−0.23	−0.39	−0.41	−0.46	−0.27
New air-sea	–	0.30	0.00	−0.05	−0.10	0.08	0.13	−0.13	−0.07	0.05
WAM C4	0.010	0.55	−0.12	−0.15	−0.23	−0.01	0.04	−0.12	−0.11	0.06
Uncoupled	0.0125	0.40	−0.06	−0.13	−0.20	0.00	0.05	−0.16	−0.12	0.02
WAM C4	0.0060	0.57	−0.14	−0.15	−0.24	−0.01	0.01	−0.14	−0.13	0.04
Regression	0.010	1.00	−0.50	−0.34	−0.48	−0.22	−0.39	−0.41	−0.46	−0.28
	$\hat{\alpha}$	ψ_{dis}	*SD*				*SD*			
WAM C4	0.010	1.00	0.31	0.24	0.25	0.26	0.45	0.31	0.39	0.30
Uncoupled	0.035	1.00	0.31	0.24	0.25	0.26	0.44	0.30	0.39	0.29
New air-sea	–	0.30	0.31	0.24	0.23	0.25	0.46	0.29	0.38	0.28
WAM C4	0.010	0.55	0.34	0.27	0.25	0.31	0.47	0.31	0.34	0.31
Uncoupled	0.0125	0.40	0.31	0.25	0.24	0.27	0.46	0.30	0.38	0.27
WAM C4	0.0060	0.57	0.32	0.27	0.25	0.30	0.45	0.31	0.34	0.31
Regression	0.010	1.00	0.31	0.24	0.25	0.26	0.45	0.31	0.39	0.30
	$\hat{\alpha}$	ψ_{dis}	*RMS*				*RMS*			
WAM C4	0.010	1.00	0.58	0.40	0.53	0.33	0.58	0.50	0.59	0.39
Uncoupled	0.035	1.00	0.59	0.42	0.55	0.35	0.59	0.51	0.60	0.40
New air-sea	–	0.30	0.31	0.24	0.26	0.27	0.48	0.32	0.39	0.28
WAM C4	0.010	0.55	0.36	0.31	0.35	0.31	0.47	0.34	0.36	0.32
Uncoupled	0.0125	0.40	0.32	0.28	0.31	0.27	0.46	0.34	0.40	0.27
WAM C4	0.0060	0.57	0.35	0.30	0.35	0.30	0.45	0.34	0.37	0.32
Regression	0.010	1.00	0.59	0.41	0.55	0.34	0.59	0.51	0.60	0.41

Table 8: *Bias, standard deviation and root-mean-square of the modelling error of H_s obtained by the (tuned) WAM Cycle 4 model, the tuned uncoupled air-sea model and the tuned new air-sea coupling module at each station for validation time periods Nov/Dec '97 and Jan '98.*

f_p [Hz]			Dec '98			
			AUK	EURO	K13	IJM
	$\hat{\alpha}$	ψ_{dis}	*BIAS*			
WAM C4	0.010	1.00	−0.54	−0.35	−0.40	−0.33
Uncoupled	0.035	1.00	−0.57	−0.38	−0.44	−0.37
New air-sea	–	0.30	−0.23	−0.10	−0.14	−0.11
WAM C4	0.010	0.55	−0.24	−0.16	−0.18	−0.11
Uncoupled	0.0125	0.40	−0.12	−0.06	−0.08	−0.04
WAM C4	0.0060	0.57	−0.24	−0.15	−0.17	−0.10
Regression	0.010	1.00	−0.52	−0.33	−0.39	−0.33
	$\hat{\alpha}$	ψ_{dis}	*SD*			
WAM C4	0.010	1.00	0.72	0.70	0.59	0.59
Uncoupled	0.035	1.00	0.75	0.75	0.62	0.62
New air-sea	–	0.30	0.76	0.74	0.64	0.60
WAM C4	0.010	0.55	0.78	0.76	0.69	0.65
Uncoupled	0.0125	0.40	0.79	0.78	0.67	0.65
WAM C4	0.0060	0.57	0.75	0.73	0.67	0.63
Regression	0.010	1.00	0.74	0.73	0.60	0.61
	$\hat{\alpha}$	ψ_{dis}	*RMS*			
WAM C4	0.010	1.00	0.90	0.79	0.71	0.68
Uncoupled	0.035	1.00	0.94	0.84	0.76	0.72
New air-sea	–	0.30	0.79	0.74	0.65	0.61
WAM C4	0.010	0.55	0.81	0.77	0.71	0.66
Uncoupled	0.0125	0.40	0.79	0.78	0.68	0.65
WAM C4	0.0060	0.57	0.78	0.75	0.69	0.64
Regression	0.010	1.00	0.90	0.81	0.72	0.69

Table 9: *Bias, standard deviation and root-mean-square of the modelling error of f_p obtained by the (tuned) WAM Cycle 4 model, the tuned uncoupled air-sea model and the tuned new air-sea coupling module at each station for tuning time period Dec '98.*

f_p [Hz]			Nov/Dec '97				Jan '98			
			AUK	EURO	K13	IJM	AUK	EURO	K13	IJM
	$\hat{\alpha}$	ψ_{dis}	*BIAS*				*BIAS*			
WAM C4	0.010	1.00	−0.79	−0.44	−0.69	−0.51	−0.61	−0.41	−0.43	−0.47
Uncoupled	0.035	1.00	−0.83	−0.42	−0.68	−0.50	−0.68	−0.46	−0.48	−0.51
New air-sea	–	0.30	−0.42	−0.11	−0.33	−0.18	−0.31	−0.29	−0.26	−0.31
WAM C4	0.010	0.55	−0.51	−0.21	−0.45	−0.29	−0.33	−0.27	−0.24	−0.28
Uncoupled	0.0125	0.40	−0.38	−0.07	−0.31	−0.14	−0.28	−0.22	−0.18	−0.22
WAM C4	0.0060	0.57	−0.50	−0.24	−0.46	−0.29	−0.32	−0.25	−0.23	−0.27
Regression	0.010	1.00	−0.79	−0.42	−0.66	−0.50	−0.63	−0.43	−0.44	−0.48
	$\hat{\alpha}$	ψ_{dis}	*SD*				*SD*			
WAM C4	0.010	1.00	1.14	0.79	0.66	0.91	0.66	0.63	0.51	0.62
Uncoupled	0.035	1.00	1.13	0.86	0.67	0.90	0.68	0.65	0.52	0.65
New air-sea	–	0.30	1.04	0.79	0.68	0.92	0.67	0.58	0.52	0.60
WAM C4	0.010	0.55	1.09	0.81	0.65	0.88	0.67	0.60	0.52	0.59
Uncoupled	0.0125	0.40	1.08	0.87	0.70	0.90	0.67	0.65	0.57	0.63
WAM C4	0.0060	0.57	1.09	0.77	0.64	0.88	0.66	0.60	0.51	0.58
Regression	0.010	1.00	1.13	0.82	0.65	0.90	0.67	0.64	0.51	0.63
	$\hat{\alpha}$	ψ_{dis}	*RMS*				*RMS*			
WAM C4	0.010	1.00	1.38	0.90	0.96	1.04	0.90	0.75	0.66	0.78
Uncoupled	0.035	1.00	1.40	0.96	0.95	1.03	0.96	0.80	0.71	0.83
New air-sea	–	0.30	1.12	0.80	0.76	0.94	0.74	0.65	0.58	0.67
WAM C4	0.010	0.55	1.20	0.84	0.79	0.93	0.75	0.66	0.57	0.65
Uncoupled	0.0125	0.40	1.15	0.87	0.77	0.91	0.72	0.69	0.60	0.67
WAM C4	0.0060	0.57	1.20	0.81	0.79	0.93	0.73	0.65	0.56	0.64
Regression	0.010	1.00	1.38	0.92	0.93	1.03	0.91	0.77	0.68	0.79

Table 10: *Bias, standard deviation and root-mean-square of the modelling error of f_p obtained by the (tuned) WAM Cycle 4 model, the tuned uncoupled air-sea model and the tuned new air-sea coupling module at each station for validation time periods Nov/Dec '97 and Jan '98.*

original WAM model with respect to H_s and f_p for each time period. Especially the biases of the modelling errors of H_s and f_p are reduced considerably, the standard deviation remains more or less the same. The tuned new air-sea module performs slightly better than the tuned WAM Cycle 4 model with respect to H_s and f_p, whereas the latter one estimates the extreme wave heights more accurately.

The tuned WAM Cycle 4 models ($\psi_{\text{dis}} = 0.55$) and ($\hat{\alpha} = 0.0060$, $\psi_{\text{dis}} = 0.57$) perform significantly better than the original WAM model with respect to H_s and f_p, especially the bias of their modelling errors is reduced for each time period. Both tuned WAM Cycle 4 models perform equally accurate, the profit gained by the additional tuning of the Charnock constant is restricted to a reduced bias for f_p.

Comparison of the results obtained by the tuned uncoupled air-sea modules ($\alpha = 0.035$) and ($\alpha = 0.0125$, $\psi_{\text{dis}} = 0.40$) leads to the remark that the latter model produces most accurate output data of H_s and f_p for each time period. Especially the bias is reduced, the standard deviation of the modelling error remains approximately the same. It shows that the influence of tuning of the strenght of the dissipation source term is more important than tuning the Charnock constant in the uncoupled air-sea parameterization.

The three different air-sea coupling modules can be intercompared by considering the tuned new air-sea coupling module ($\psi_{\text{dis}} = 0.30$), the tuned uncoupled air-sea model ($\alpha = 0.0125$, $\psi_{\text{dis}} = 0.40$) and the tuned WAM Cycle 4 model ($\hat{\alpha} = 0.0060$, $\psi_{\text{dis}} = 0.57$). It is clear that each of them performs better than the original WAM Cycle 4 model, especially the bias of the modelling errors of H_s and f_p is reduced, whereas the standard deviation remains approximately the same. The three tuned air-sea coupling modules perform equally accurate, the tuned WAM Cycle 4 model estimates the extreme wave heights most accurately. It is difficult to conclude which one to prefer above the other as there appears to be no structural relation between the accuracy of the model output, wave parameters, observation stations, time period or type of weather.

The wind input analysis performed in Section 4.2 shows in Tables 3 and 5 that the modelled input wind velocities at several stations (AUK and IJM) are over-estimated, while those at other stations are under-estimated. Because the wave height is directly influenced by the wind velocity, it is expected that the wave models produce consistent over- and under-estimations of H_s at the corresponding stations. The calculated statistics of the modelling errors of H_s in Tables 7 and 8 show that this concistency does not hold for the original WAM Cycle 4 model and the tuned uncoupled air-sea model ($\alpha = 0.035$), reflected by the negative biases of the modelling errors of H_s at AUK and IJM. The remaining tuned air-sea coupling modules show this consistency only for time period Jan '98. During the other time periods, the tuned new air-sea coupling module is the only one producing wave heights that are consistent to the winds, which is an advantage of this coupling routine over the other coupling schemes.

4.4.2 Various scatter plots and time series

The performance of the three alternative air-sea coupling modules is assessed by studying various scatter plots and time series concerning the drag coefficient, air-sea coupling parameter and Charnock parameter which are derived from the wave model output. In this section only the output of the WAM model runs performed by the original WAM Cycle 4 model, the tuned uncoupled air-sea scheme ($\alpha = 0.035$) and the tuned new air-sea coupling parameterization ($\psi_{\text{dis}} = 0.30$) is used.

Figure 8 shows scatter plots of calculated drag coefficient $C_D = u_*^2/U_{10}^2$ versus wind

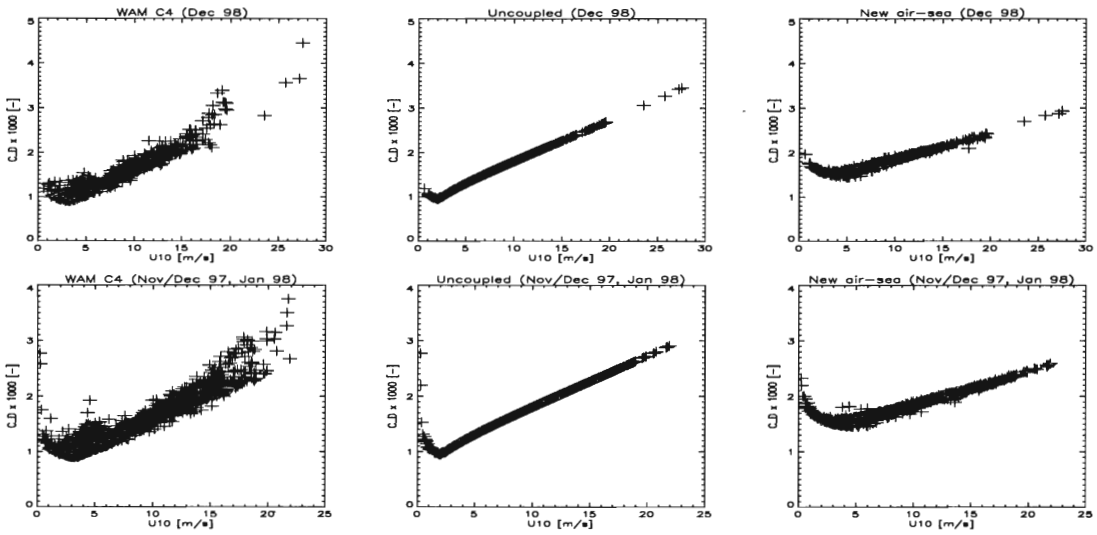

Figure 8: *Drag coefficient C_D versus U_{10} obtained by the WAM Cycle 4 model, the tuned uncoupled air-sea model and the tuned new air-sea coupling module at the four observation stations for tuning time period Dec '98 and validation time periods Nov/Dec '97 - Jan '98.*

velocity U_{10} for each coupling module for the tuning time period and both validation time periods. It is obvious that the original WAM Cycle 4 model produces more scatter of the calculated C_D compared to the tuned new coupling module. The plots for the tuned new air-sea coupling module suggest a direct relation between C_D and U_{10}. All coupling modules show an increasing tendency of C_D for large values of U_{10}. This increase is less steep for the new coupling module than for the original WAM Cycle 4 model, which covers a somewhat broader range of C_D values.

Figures 17-19 in Appendix A.3 show the time series of calculated numerical coupling parameter y for the original WAM Cycle 4 model and for the tuned new air-sea coupling module for each observation station and all time periods. It is apperent that the coupling parameters calculated by the tuned new air-sea parameterization are smaller, covering a smaller range of values, than those used by the original WAM Cycle 4 model.

The relative cumulative frequency distribution obtained by each air-sea coupling model is displayed for each station in Figure 9. It represents the relative number of times a certain value of coupling parameter y is used during the WAM model run at the corresponding station during the three time periods. The displayed cumulative distributions show a rapid increase for those values of the coupling parameter which are often calculated during the model runs. It is clear that the tuned new air-sea coupling module uses lower values of y, while both tuned WAM Cycle 4 models use higher values of y, also near the critical discontinuity value 1, compared to the original WAM Cycle 4 model.

The scatter plots of calculated coupling parameter versus wind velocity U_{10} are presented in the four most right pictures in Figure 10 for the WAM Cycle 4 model and the tuned new coupling module. They show that the WAM Cycle 4 model produces much more scatter of the coupling parameter within a broader range compared to the new coupling module. Both modules show an increasing tendency between the coupling parameter and U_{10}. The values of y obtained by WAM Cycle 4 are mainly located at value 0.8, while those obtained by the

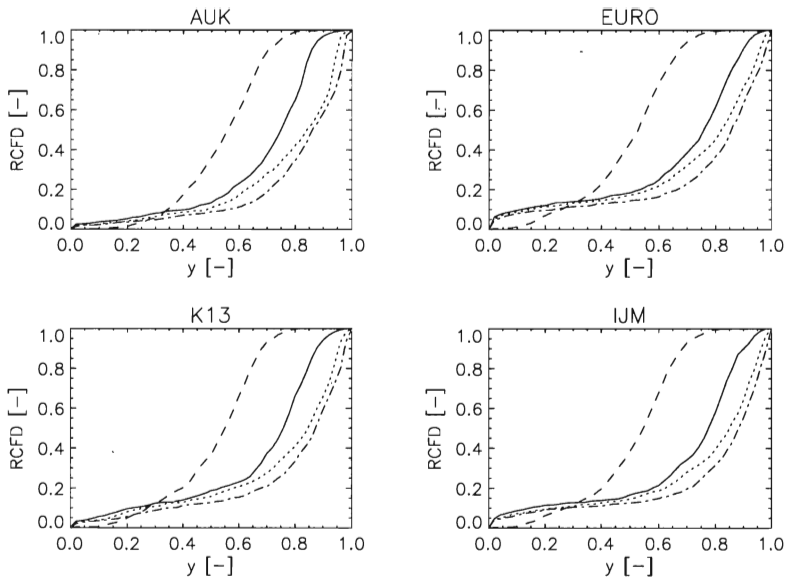

Figure 9: *Relative cumulative frequency distribution of the coupling parameter for the WAM Cycle 4 model (—), tuned new air-sea coupling module (−−), tuned WAM Cycle 4 model ($\psi_{\text{dis}} = 0.55$) (· · ·) and tuned WAM Cycle 4 model ($\hat{\alpha} = 0.0060$, $\psi_{\text{dis}} = 0.57$) (− · −) for tuning time period Dec '98 and validation time periods Nov/Dec '97 - Jan '98.*

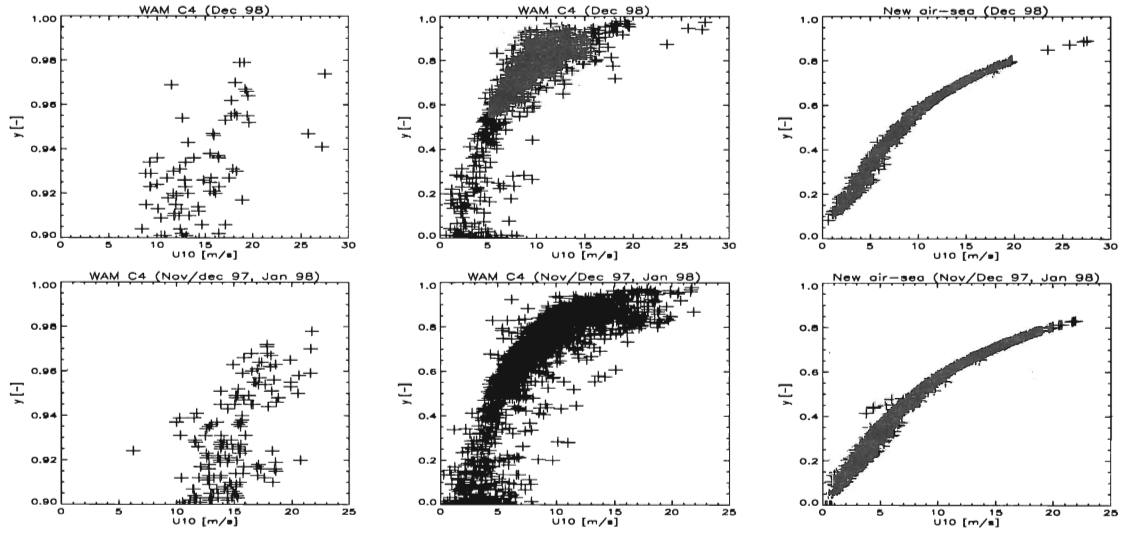

Figure 10: *Coupling parameter y versus U_{10} obtained by the WAM Cycle 4 model (limited for $0.9 \leq y \leq 1.0$ on the two left figures) and the tuned new air-sea coupling module for tuning time period Dec '98 and validation time periods Nov/Dec '97 - Jan '98.*

new coupling module are smaller and more evenly distributed for U_{10}. The numerical limiter described by (18) is not applied for the performed calculations of the WAM Cycle 4 model. The two left most pictures in Figure 10 show the scatter plots of coupling parameter y of the WAM Cycle 4 model versus U_{10} for the limited range $0.9 \leq y \leq 1.0$. It is found that $y \leq 0.98$ for the WAM Cycle 4 model and $y < 0.89$ for the new coupling module for all time periods.

The numerical limiter L of (22) is introduced in the original WAM Cycle 4 model for numerical stability reasons. It is also applied in the tuned uncoupled air-sea model and the tuned new air-sea coupling module, although it is not directly related to the parameterization of the air-sea interaction process. The impact of numerical limiter L is assessed by studying ratio ε defined in (24). The time series of ratio ε for the three alternative coupling modules are presented in Figures 20-22 of Appendix A.4. The limiter is not applied if $\varepsilon = 1$, but smaller values $\varepsilon < 1$ mean a larger impact of the limiter on the calculated spectral solution. The time series of ε for the WAM Cycle 4 model and the tuned uncoupled air-sea model are similar. They show much more and much larger peaks of $\varepsilon < 1$ compared to the time series of the tuned new air-sea coupling module. This means that the limiter is more frequently applied and causing a larger impact on the numerical spectral solution by the original WAM Cycle 4 model compared to the new air-sea coupling module. Although this limiter is not directly connected to the air-sea coupling scheme, the new air-sea coupling module apperently generates a numerically more stable scheme with regard to this limiter.

5 Summary and conclusions

This report assesses three alternative parameterizations of the air-sea interaction in the WAM wave model. The first describes the original air-sea coupling of WAM Cycle 4 by Janssen (1989, 1991), the second uncouples the sea state influence on the wind profile and the third describes a new air-sea coupling module presented by Makin and Kudryavtsev (1999). Both physics and numerics of these coupling schemes are discussed.

Several drawbacks of the air-sea coupling in the original WAM Cycle 4 model are stressed, concerning the use of the Charnock relation to describe the roughness length and the parameterization of the growth rate by Miles theory. Besides that, the inconsistent numerical implementation of the coupling parameter and the use of a pre-described high-frequency tail of Phillips are mentioned. The new air-sea coupling module applies a modern advanced parameterization. It calculates the fluxes directly, the Charnock relation and the concept of roughness length are not used and the new growth rate parameterization is based on rapid distortion theory of turbulence above waves. Besides that, the high-frequency tail is accurately approximated and the coupling is complete by a consistent numerical implementation. These alternative air-sea parameterizations are developed, coded and implemented into the WAM model.

An iterative parameter tuning algorithm is developed based on a finite difference approach together with the Levenberg-Marquardt optimization method, which efficiently combines the method of steepest descent and the method of Newton. It minimizes a cost-function representing the misfit between calculated wave model data and North Sea buoy observations. This parameter tuning method is coded and implemented. It is applied to tune the Charnock constant in the original and uncoupled air-sea parameterization and/or the energy dissipation function against one of the three air-sea coupling modules with respect to several wave parameters at four stations during a time period of one month. The tuned modules are validated and intercompared by using the North Sea buoy wave observations of two independent time periods.

It is noted, that the coupling modules are tuned especially for the North Sea area in the current studies, which is, in contrast to a deep ocean, a shallow sea containing an influential bathymetry. Application of the various wave models to an ocean, sea or lake different from the North Sea requires a re-tuning of the control parameters by taking into account wave parameter observations of that particular area.

Firstly, it is concluded that the original WAM Cycle 4 model produces equally accurate wave heights and peak frequencies compared to the uncoupled air-sea module using a tuned fixed Charnock constant, or compared to the module that replaces the coupling parameter by a pre-described regression curve. It shows that the wind and the waves are not fully coupled by the numerical scheme of the original WAM Cycle 4 model. The use of the dynamic computationally expensive coupling parameter is not obvious.

The WAM Cycle 4 model produces structural under-estimations of the wave heights and peak frequencies. Tuning the several (new) air-sea parameterizations leads to a considerably reduced overall strength of the wave energy dissipation which restores these under-estimations by reducing the biases of the modelling errors of these wave parameters. Their standard deviations are not reduced, however.

The WAM Cycle 4 model and the uncoupled air-sea model, tuned for both the Charnock parameter and the dissipation strength, and the new air-sea interaction module, tuned for the dissipation strength, produce more accurate wave heights and peak frequencies than the

original untuned WAM Cycle 4 model. The biases of the modelling errors of these wave parameters are reduced, but their standard deviations are not. The tuned original model produces more accurate extreme wave heights compared to the other models.

A more consistent relation between the wind input fields and the modelled wave heights is obtained by the tuned new air-sea interaction scheme. Besides that, the tuned new air-sea coupling module produces little scatter between various wave parameters, it uses smaller values of the coupling parameter avoiding possible singularities and it is shown to be more numerically stable with respect to a certain applied limiter. The numerical implementation of the physics concerning the air-sea coupling is more consistent for the new coupling parameterization.

It may be concluded that the new air-sea coupling parameterization is preferred to the original air-sea coupling scheme currently applied in the WAM Cycle 4 model. The benefits obtained by this new coupling module are marginal, however. It can be said that the air-sea coupling module applying the Charnock relation, possibly even using a fixed Charnock constant, suffices the purpose of wave prediction. On the other hand, the effects of the alternative air-sea coupling modules may not be distinctly shown, caused by possible remaining numerical artifacts in the WAM model concerning parameterizations and numerics of wave processes other than the air-sea coupling. This may require a more detailed revision of the (numerical) WAM model.

The assessment of effects on atmospheric processes by the alternative coupling modules requires their incorporation into models which couple the ocean and the atmosphere dynamically, like ECAWOM or operational weather prediction models.

Acknowledgements

E. Bouws (KNMI) is acknowledged for delivering and reviewing the North Sea wave observation data sets. J.R.A. Onvlee (KNMI) and R. Weisse (GKSS) are thanked for providing several useful comments, while J.F. Meirink (NWO/KNMI) is thanked for stimulating discussions. This research was supported by the EU Environment Programme (Contract ENV4-CT97-0460, ASPEN).

A Time series

A.1 Wind velocity at 10 m height

Tuning period Dec '98:

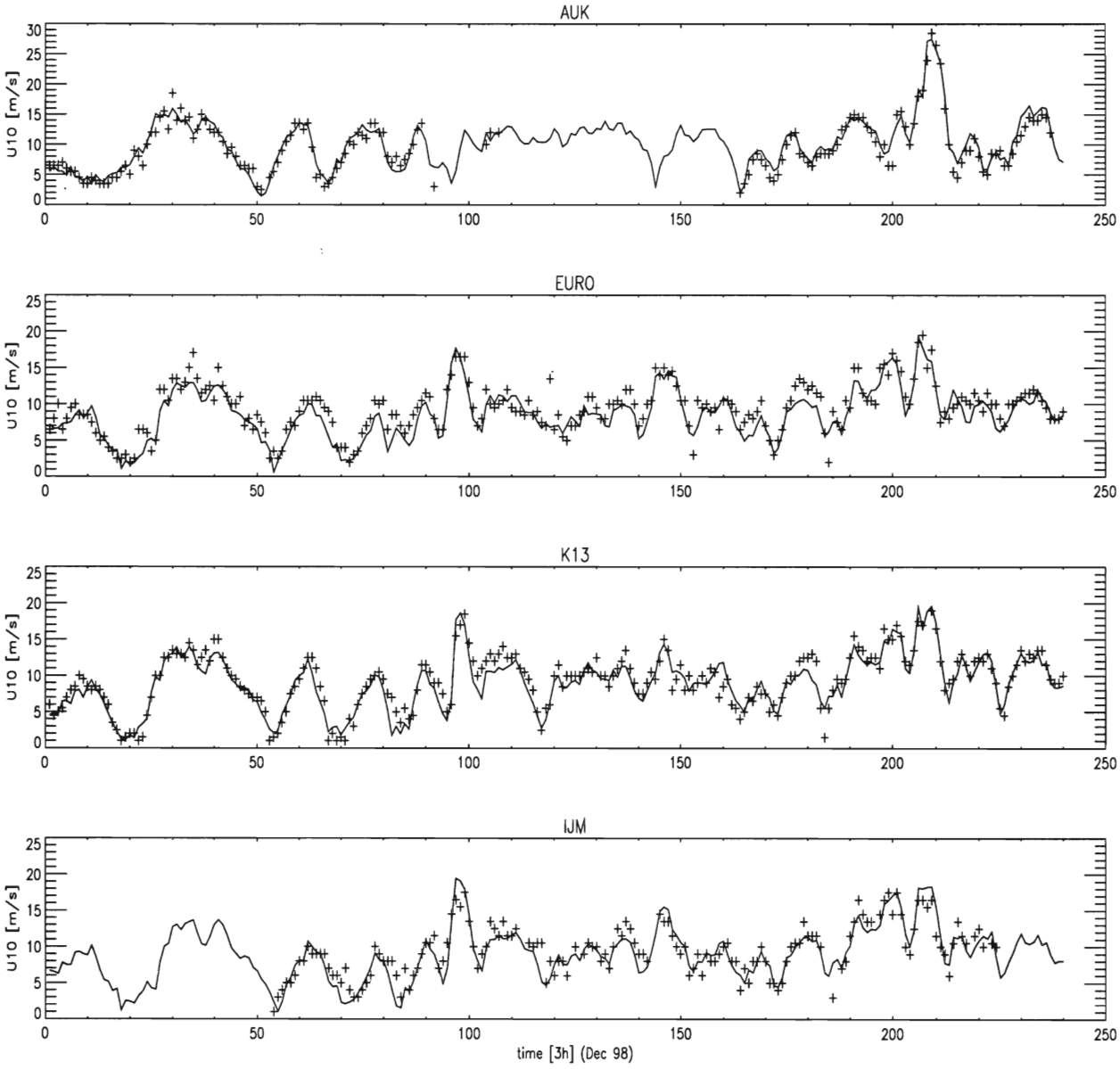

Figure 11: *Calculated U_{10} according to HIRLAM after interpolation (—) and observations U_{10}^{obs} (+) for tuning time period Dec '98 at each observation station.*

Validation period Nov/Dec '97:

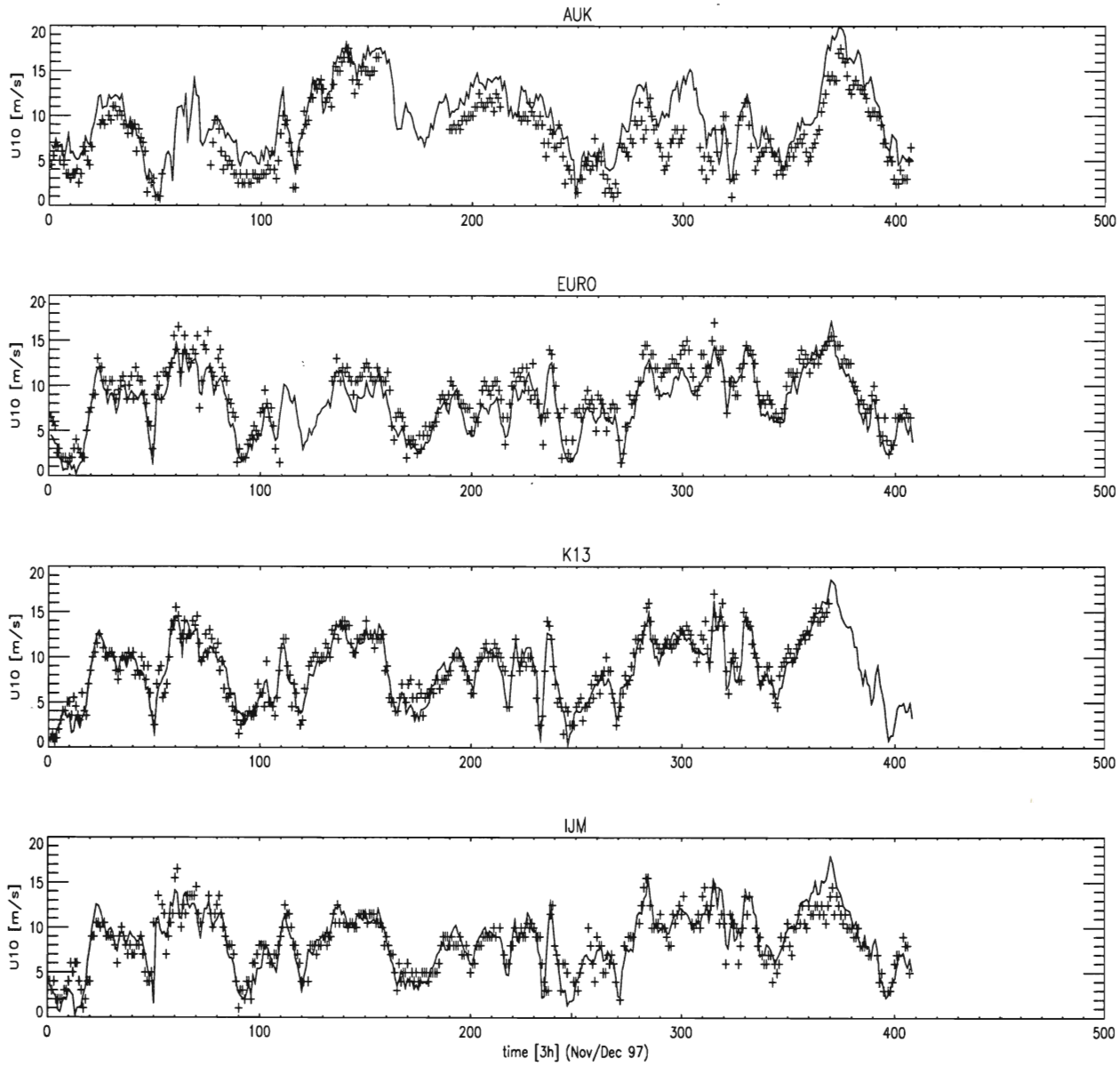

Figure 12: *Calculated U_{10} according to HIRLAM after interpolation (—) and observations U_{10}^{obs} (+) for validation period Nov/Dec '97 at each observation station.*

Validation period Jan '98:

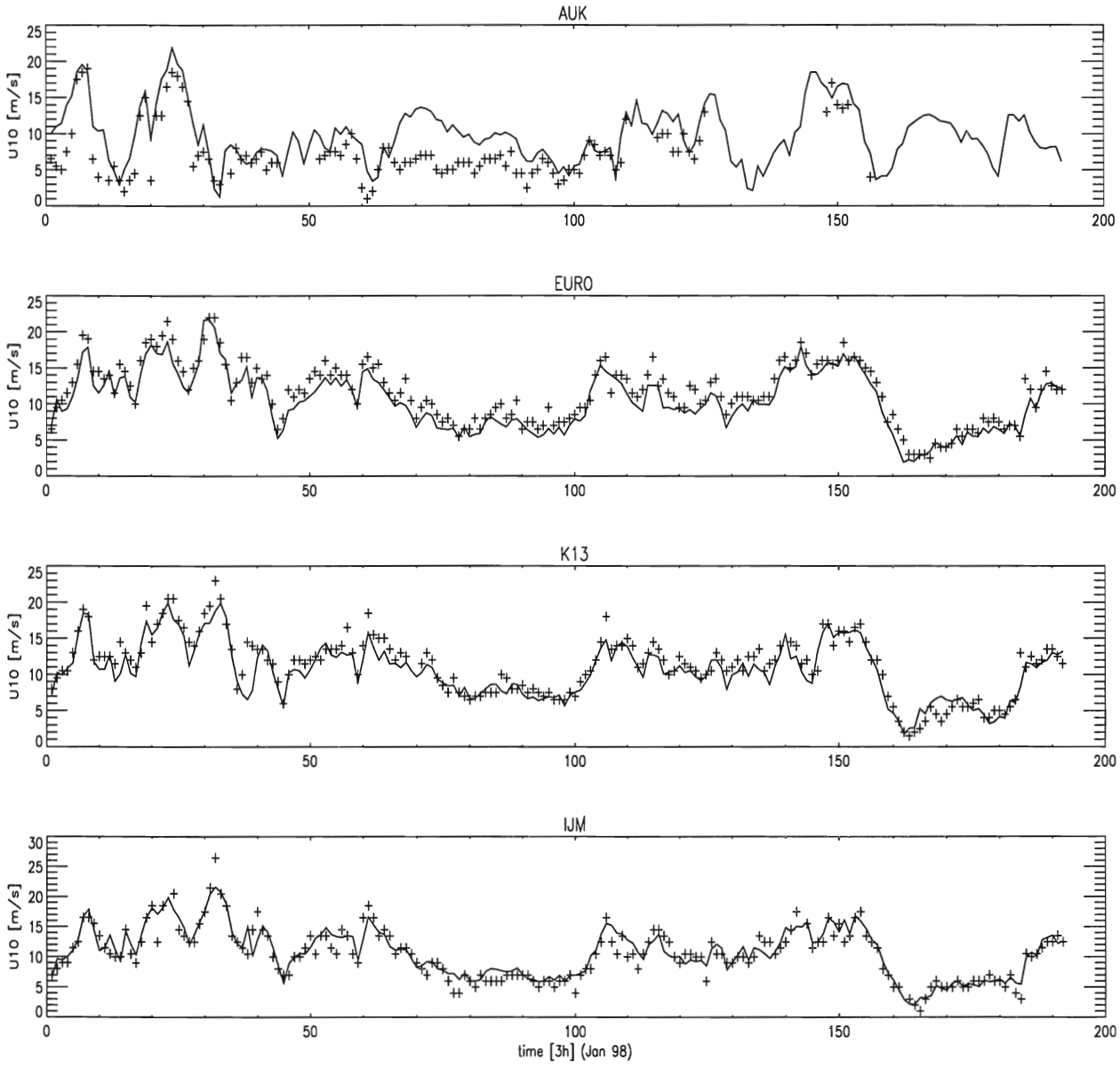

Figure 13: *Calculated U_{10} according to HIRLAM after interpolation (—) and observations U_{10}^{obs} (+) for validation time period Jan '98 at each observation station.*

A.2 Significant wave height

Tuning period Dec '98:

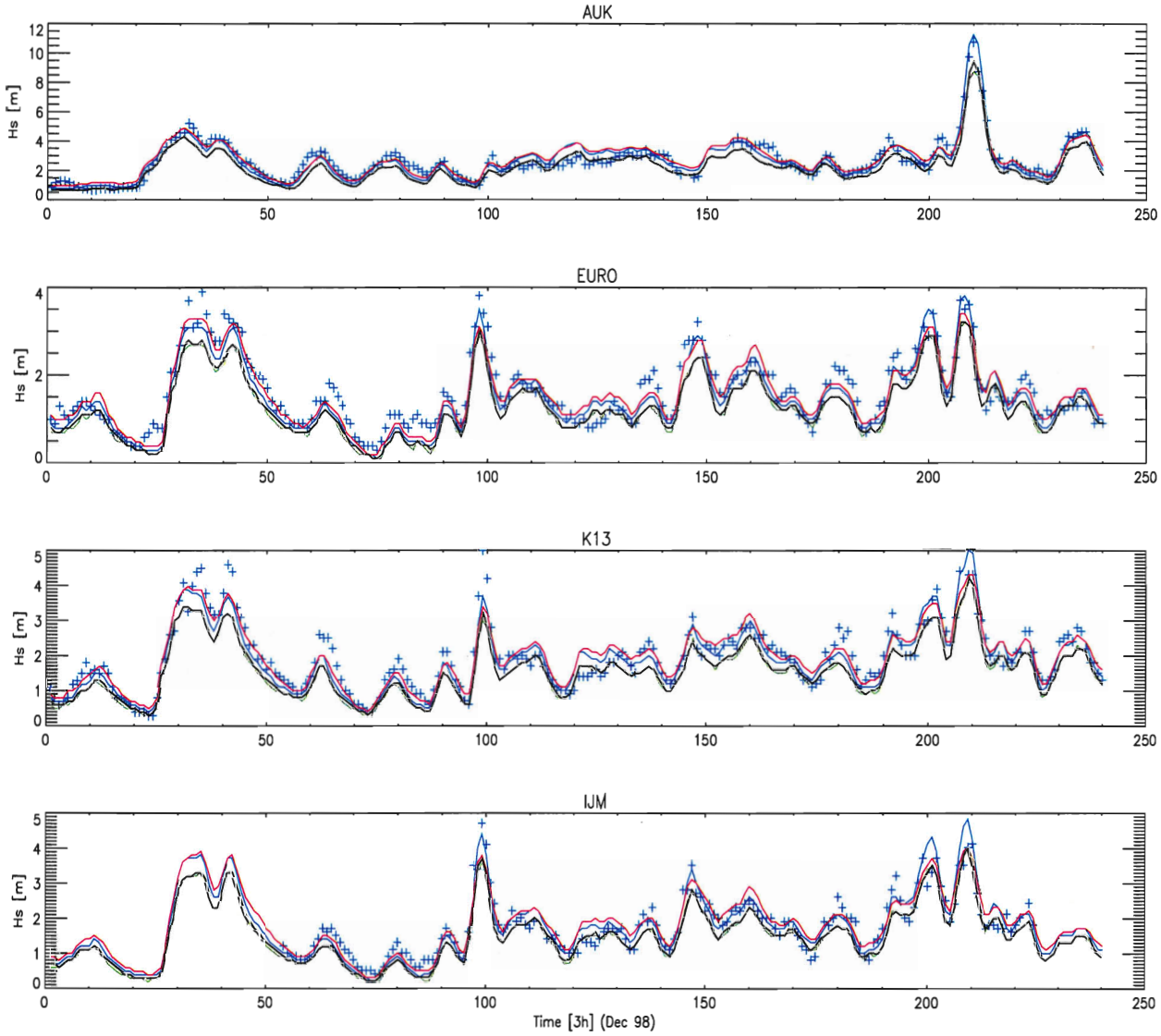

Figure 14: *Calculated H_s according to the original WAM Cycle 4 model ($\hat{\alpha} = 0.01$, $\psi_{\rm dis} = 1.0$) (black), tuned uncoupled air-sea model ($\alpha = 0.035$) (green), tuned new air-sea coupling module ($\psi_{\rm dis} = 0.30$) (red), tuned WAM Cycle 4 model ($\psi_{\rm dis} = 0.55$) (blue), and observations $H_s^{\rm obs}$ (+) for tuning time period Dec '98 at each observation station.*

Validation period Nov/Dec '97:

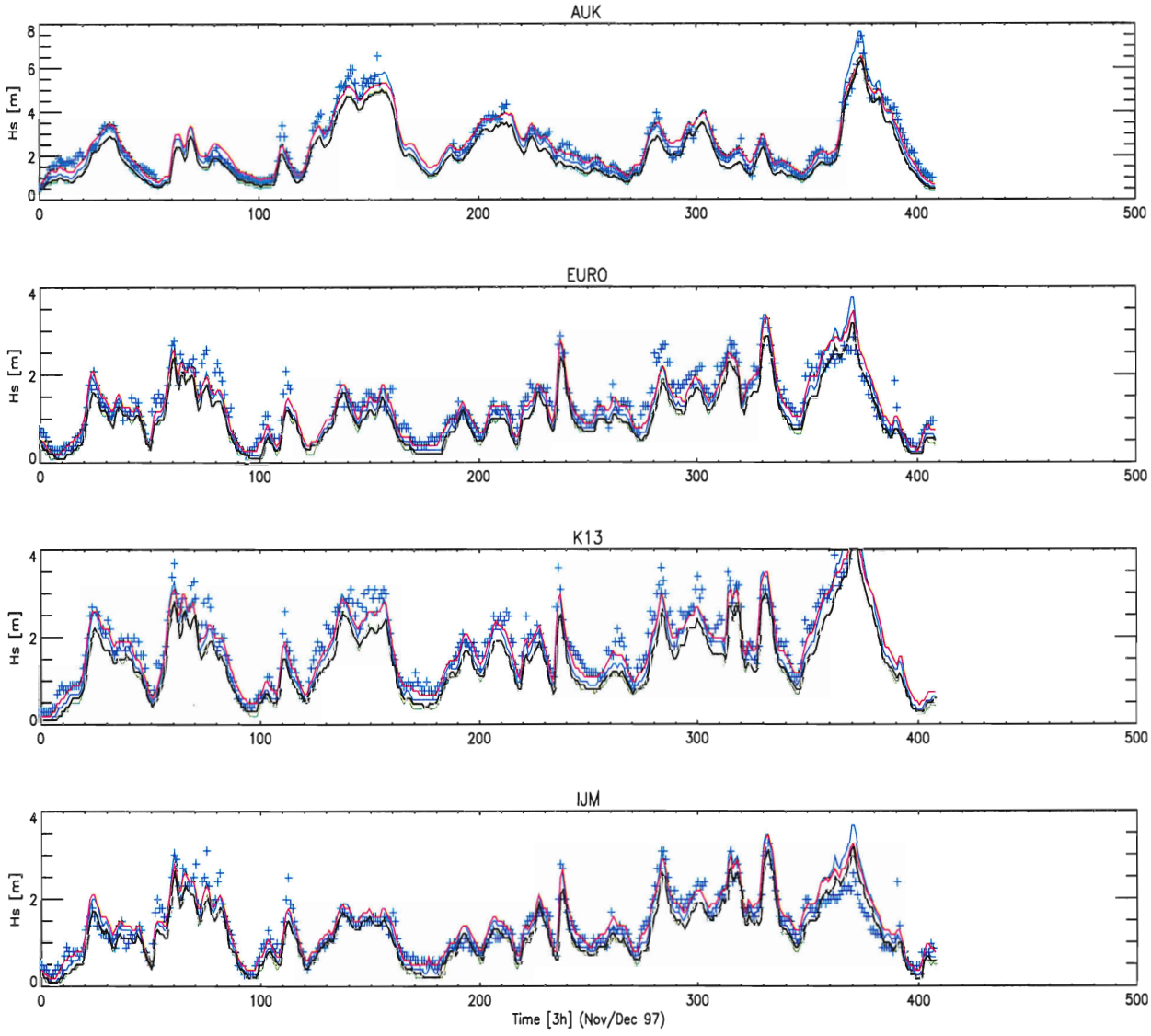

Figure 15: *Calculated H_s according to the original WAM Cycle 4 model ($\hat{\alpha} = 0.01$, $\psi_{\text{dis}} = 1.0$) (black), tuned uncoupled air-sea model ($\alpha = 0.035$) (green), tuned new air-sea coupling module ($\psi_{\text{dis}} = 0.30$) (red), tuned WAM Cycle 4 model ($\psi_{\text{dis}} = 0.55$) (blue), and observations H_s^{obs} (+) for validation time period Nov/Dec '97 at each observation station.*

Validation period Jan '98:

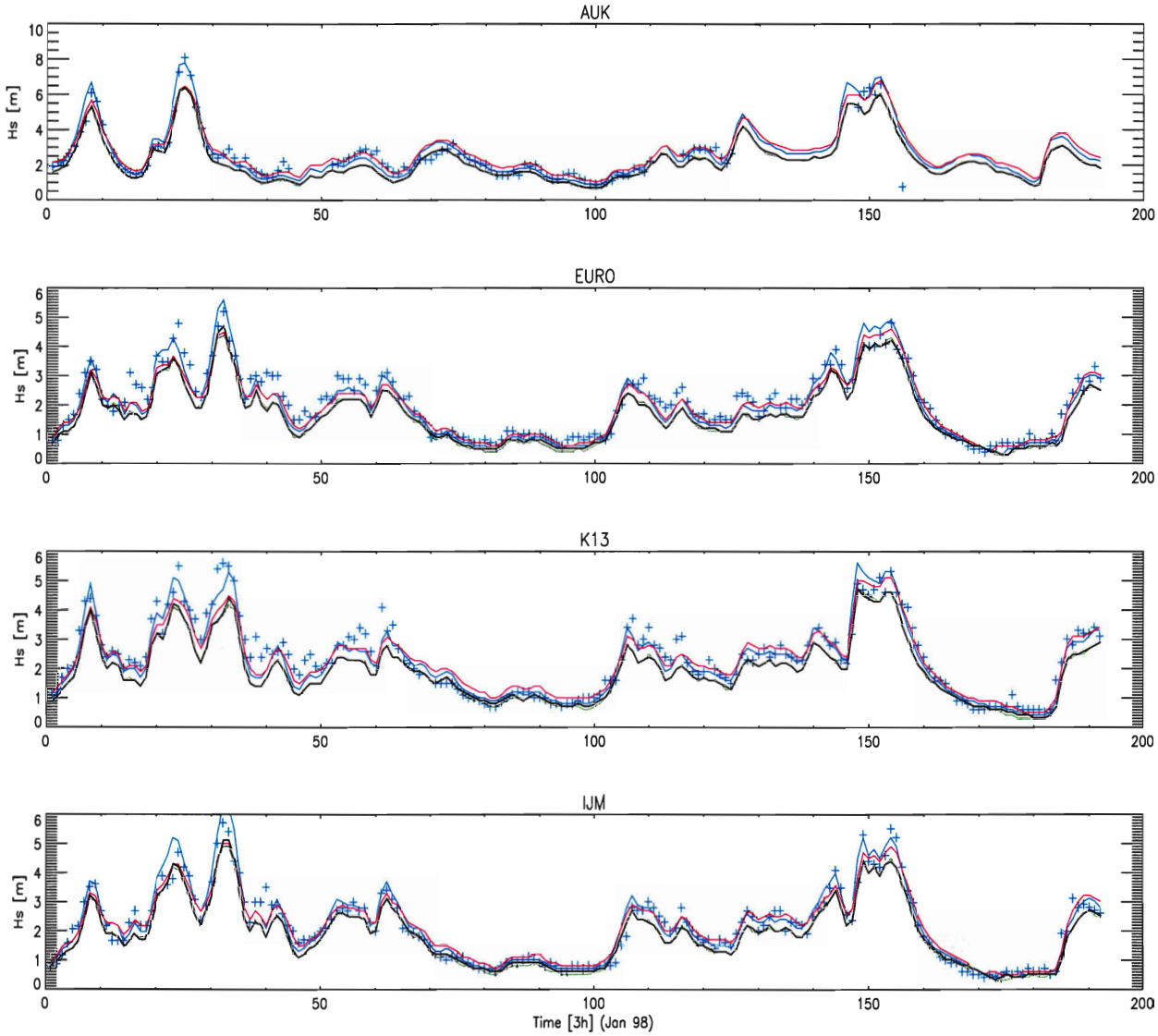

Figure 16: *Calculated H_s according to the original WAM Cycle 4 model ($\hat{\alpha} = 0.01$, $\psi_{\rm dis} = 1.0$) (black), tuned uncoupled air-sea model ($\alpha = 0.035$) (green), tuned new air-sea coupling module ($\psi_{\rm dis} = 0.30$) (red), tuned WAM Cycle 4 model ($\psi_{\rm dis} = 0.55$) (blue), and observations $H_s^{\rm obs}$ (+) for validation time period Jan '98 at each observation station.*

A.3 Air-sea coupling parameter

Tuning period Dec '98:

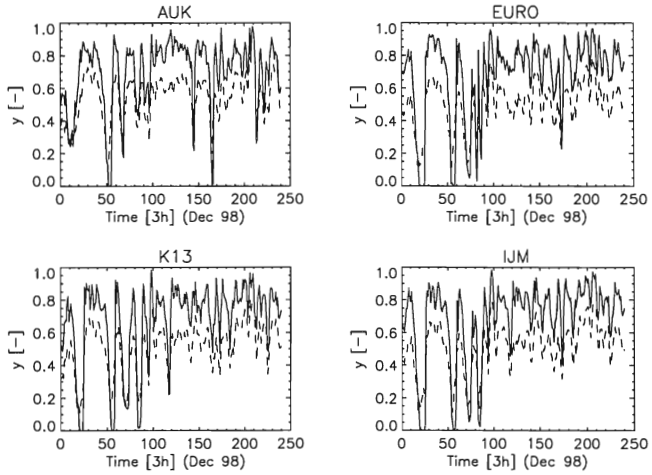

Figure 17: *Coupling parameter y for the original WAM Cycle 4 model (—) and the tuned new air-sea coupling module (−−) at each observation station for tuning time period Dec '98.*

Validation period Nov/Dec '97:

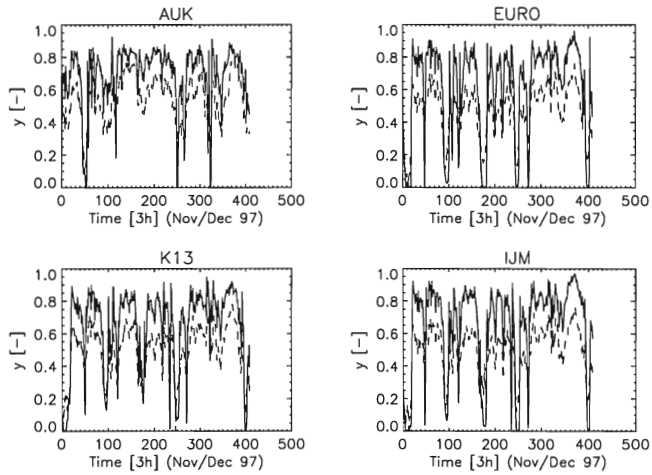

Figure 18: *Coupling parameter for the original WAM Cycle 4 model (—) and the tuned new air-sea coupling module (−−) at each observation station for validation time period Nov/Dec '97.*

Validation period Jan '98:

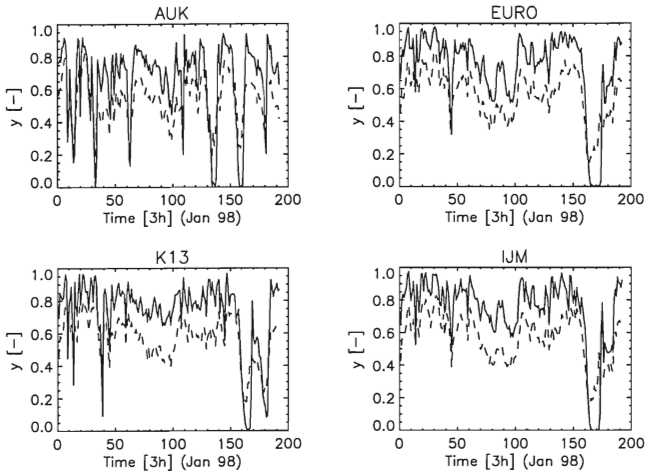

Figure 19: *Coupling parameter for the original WAM Cycle 4 model (—) and the tuned new air-sea coupling module (−−) at each observation station for validation time period Jan '98.*

A.4 Numerical limiter

Tuning period Dec '98:

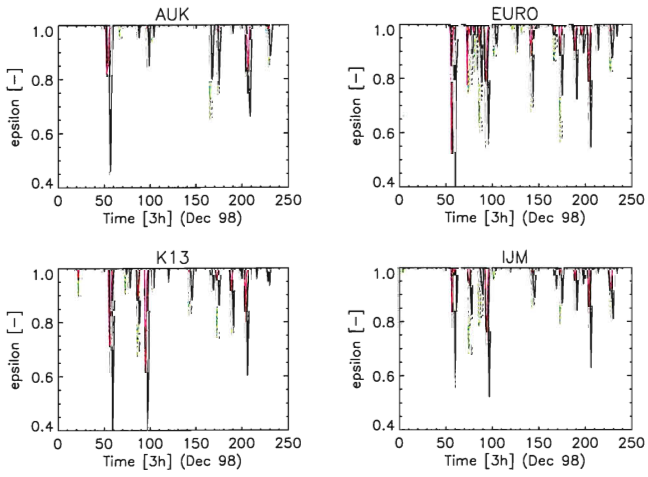

Figure 20: *Ratio ε describing the impact of the limiter in the original WAM Cycle 4 model (black), the tuned uncoupled air-sea model (green) and the tuned new air-sea coupling module (red) at each observation station for tuning time period Dec '98.*

Validation period Nov/Dec '97:

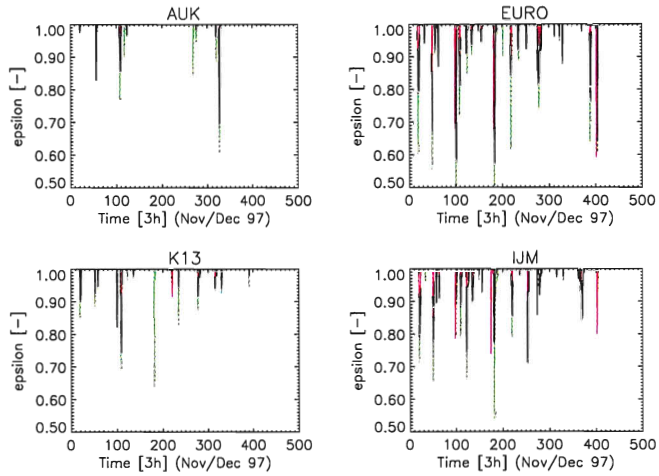

Figure 21: *Ratio ε describing the impact of the limiter in the original WAM Cycle 4 model (black), the tuned uncoupled air-sea model (green) and the tuned new air-sea coupling module (red) at each observation station for validation time period Nov/Dec '97.*

Validation period Jan '98:

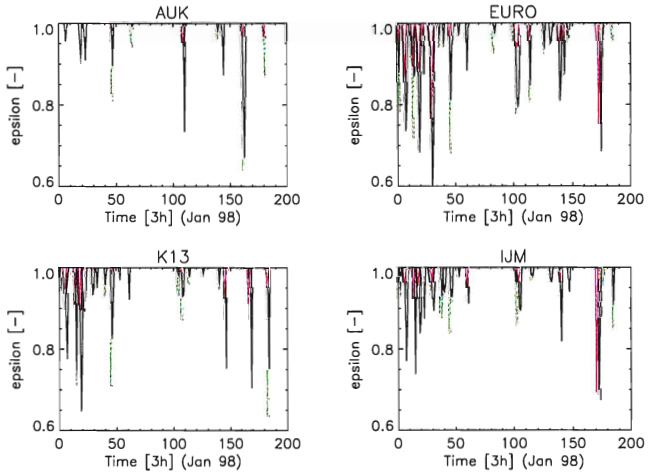

Figure 22: *Ratio ε describing the impact of the limiter in the original WAM Cycle 4 model (black), the tuned uncoupled air-sea model (green) and the tuned new air-sea coupling module (red) at each observation station for validation time period Jan '98.*

References

Belcher, S.E. and J.C.R. Hunt (1993): *Turbulent shear flow over slowly moving waves*, J. Fluid. Mech. **251**, pp. 109-148.

Benschop, H. (1996): *Windsnelheidsmetingen op zeestations en kuststations: herleiding waarden windsnelheid naar 10-meter niveau*, Technical Report TR-188, Royal Netherlands Meteorological Institute (KNMI), De Bilt (in Dutch).

Burgers, G. (1990): *A guide to the Nedwam wave model*, Scientific Report WR-90-04, Royal Netherlands Meteorological Institute (KNMI), De Bilt.

Charnock, H. (1955): *Wind stress on a water surface*, Q.J.R. Meteorol. Soc. **81**, pp. 639-640.

Elfouhaily, T., B. Chapron, K.B. Katsaros and D. Vandemark (1997): *A unified directional spectrum for long and short wind-driven waves*, J. Geophys. Res. **102**, pp. 15,781-15,796.

Günther, H.,S. Hasselmann and P.A.E.M. Janssen (1992): *WAM model Cycle 4 (revised version)*, Technical Report No. 4, German Climate Computer Center (DKRZ), Hamburg.

Hersbach, H. (1997): *The adjoint of the WAM model*, Scientific Report WR 97-01, Royal Netherlands Meteorological Institute (KNMI), De Bilt.

Hersbach H. (1998): *Application of the adjoint of the WAM model to inverse wave modelling*, J. Geophys. Res. **103**, pp. 10,469-10,487.

Holthuijsen, L.H., N. Booij, M. van Endt, S. Caires and C. Guedes Soares (1996): *Assimilation of buoy and satellite data in wave forecasts with integral control variabels*, J. Mar. Syst. **13**, pp. 21-31.

Janssen, P.A.E.M. (1989): *Wave-Induced Stress and the Drag of Air Flow over Sea Waves*, J. Phys. Oceanogr. **19**, pp. 745-754.

Janssen, P.A.E.M. (1991): *Quasi-linear Theory of Wind-Wave Generation Applied to Wave Forecasting*, J. Phys. Oceanogr. **21**, pp. 1631-1642.

Komen, G.J., L. Cavaleri, M. Donelan, K. Hasselmann, S. Hasselmann and P.A.E.M. Janssen (1994): *Dynamics and Modelling of Ocean Waves*, Cambridge University Press.

Kudryavtsev, V.N., V.K. Makin and B. Chapron (1999): *Coupled sea surface-atmosphere model (Part 2): Spectrum of short wind waves*, J. Geophys. Res. **104**, pp. 7625-7639.

Levenberg, L. (1944): *A method for the solution of certain non-linear problems in least squares*, Quart. Appl. Math. **2**, pp. 164-168.

Makin, V.K. (1998): *Air-sea exchange of heat in the presence of wind wave and spray*, J. Geophys. Res. **103**, pp. 1137-1152.

Makin, V.K. and V.N. Kudryavtsev (1999): *Coupled sea surface-atmosphere model (Part 1): Wind over waves coupling*, J. Geophys. Res. **104**, pp. 7613-7623.

Makin, V.K., V.N. Kudryavtsev and C. Mastenbroek (1995): *Drag of the sea surface*, Boundary Layer Meteorol. **73**, pp. 159-182.

Marquardt, D.W. (1963): *An algorithm for least-squares estimation of nonlinear parameters*, J. Soc. Indust. Appl. Math. **11**, pp. 431-441.

Miles, J.W. (1957): *On the generation of surface waves by shear flows*, J. Fluid. Mech **3**, pp. 185-204.

Phillips, O.M. (1958): *The equilibrium range in the spectrum of wind-generated waves*, J. Fluid. Mech **4**, pp. 426-434.

Phillips, O.M. (1977): *The Dynamics of the Upper Ocean*, (2^{nd} edition), Cambridge University Press.

Plant, W.J. (1982): *A relation between wind stress and wave slope*, J. Geophys. Res. **87**, pp. 1961-1967.

Press, W.H., S.A. Teukolsky, W.T. Vetterling and B.P. Flannery (1992): *Numerical Recipes in FORTRAN 77: The Art of Scientific Computing*, (2^{nd} edition), Cambridge University Press.

Voorrips, A. (1998): *Sequential data assimilation methods for ocean wave models*, PhD Thesis, Royal Netherlands Meteorological Institute (KNMI), De Bilt.

WAMDI Group (1988): *The WAM model - A third generation ocean wave prediction model*, J. Phys. Oceanogr. **18**, pp. 1775-1810.

Weisse, R. and E.F. Alvares (1997): *The European Coupled Atmosphere Wave Ocean Model ECAWOM*, Report No. 238, Max-Planck-Institut für Meteorologie, Hamburg.

WMO (1998): *Guide to Wave Analysis and Forecasting*, (2^{nd} edition), WMO-No. 702.

KNMI-PUBLICATIES, VERSCHENEN SEDERT 1997

Een overzicht van eerder verschenen publicaties, wordt verzoek toegezonden door de Bibliotheek van het KNMI, postbus 201, 3730 AE De Bilt, tel. 030 - 2 206 855, fax. 030 - 2 210 407; e-mail: biblioth@knmi.nl

▼ KNMI-PUBLICATIE MET NUMMER

150-28 Sneeuwdek in Nederland 1961-1990 / A.M.G. Klein Tank
180a List of acronyms in environmental sciences : revised edition / [compiled by P. Geerders and M. Waterborg]
181b FM12 SYNOP . internationale en nationale regelgeving voor het coderen van de groepen 7wwW1W2 en 960ww; derde druk
183-1 Rainfall in New Guinea (Irian Jaya) / T.B. Ridder
183-2 Vergelijking van zware regens te Hollandia (Nieuw Guinea), thans Jayapura (Irian Jaya) met zware regens te De Bilt / T. B. Ridder
183-3 Verdamping in Nieuw-Guinea, vergelijking van gemeten hoeveelheden met berekende hoeveelheden / T.B. Ridder
183-4 Beschrijving van het klimaat te Merauke, Nieuw Guinea, in verband met de eventuele vestiging van een zoutwinningsbedrijf / T.B. Ridder a.o.
183-5 Overzicht van klimatologische en geofysische publikaties betreffende Nieuw-Guinea / T.B. Ridder
184a Inleiding tot de algemene meteorologie : studie-uitgave ; 2e druk / B. Zwart, A. Steenhuisen, m.m.v. H.J. Krijnen
185a Handleiding voor het gebruik van sectie 2 van de FM 13-X SHIP-code voor waarnemers op zee / KNMI; KLu; KM
186-I Rainfall generator for the Rhine Basin: single-site generation of weather variables by nearest-neighbour resampling / T. Brandsma a.o.
186-II Rainfall generator for the Rhine Basin: multi-site generation of weather variables by nearest-neighbour resampling / T. Brandsma a.o.
186-III Rainfall generator for the Rhine Basin: nearest-neighbour resampling of daily circulation indices and conditional generation of weather variables / Jules J. Beersma and T. Adri Buishand
187 De wind in de rug: KNMI-weerman schaatst de Elfstedentocht / H. van Dorp
188 SODA workshop on chemical data assimilation: proceedings; 9-10 December 1998, KNMI, De Bilt, The Netherlands
189 Aardbevingen in Noord-Nederland in 1998: met overzichten over de periode 1986-1998 / [Afdeling Seismologie]
190 Seismisch netwerk Noord-Nederland / [afdeling Seismologie]

▼ TECHNISCH RAPPORT = TECHNICAL REPORT (TR)

174 Report of the ASGASEX'94 workshop / ed. by W.A. Oost
175 Over slecht zicht, bewolking, windstoten en gladheid / J. Terpstra
176 Verification of the WAQUA/CSM-16 model for the winters 1992-93 and 1993-94 / J.W. de Vries
177 Nauwkeuriger nettostraling meten / M.K. van der Molen en W. Kohsiek
178 Neerslag in het stroomgebied van de Maas in januari 1995: waarnemingen en verificatie van modelprognoses / R.Jilderda a.o.
179 First field experience with 600PA phased array sodar / H. Klein Baltink
180 Een Kalman-correctieschema voor de wegdektemperatuurverwachtingen van het VAISALA-model / A. Jacobs
181 Calibration study of the K-Gill propeller vane / Marcel Bottema
182 Ontwikkeling van een spectraal UV-meetinstrument / Frank Helderman
183 Rainfall generator for the Rhine catchment : a feasibility study / T. Adri Buishand and Theo Brandsma
184 Parametrisatie van mooi-weer cumulus / M.C. van Zanten
185 Interim report on the KNMI contributions to the second phase of the AERO-project / Wiel Wauben, Paul Fortuin a.o.
186 Seismische analyse van de aardbevingen bij Middelstum (30 juli 1994) en Annen (16 augustus '94 en 31 januari '95) / [Seismologisch Onderzoek]
187 Analyse wenselijkheid overname RIVM-windmeetlokaties door KNMI / H. Benschop
188 Windsnelheidsmetingen op zeestations en kuststations: herleiding waarden windsnelheden naar 10-meter niveau / H. Benschop
189 On the KNMI calibration of net radiometers / W. Kohsiek
190 NEDWAM statistics over the period October 1994 - April 1995 / F.B. Koek
191 Description and verification of the HIRLAM trajectory model / E. de Bruijn
192 Tiltmeting : een alternatief voor waterpassing ? / H.W. Haak
193 Error modelling of scatterometer, in-situ and ECMWF model winds; a calibration refinement / Ad Stoffelen
194 KNMI contribution to the European project POPSICLE / Theo Brandsma a.o.
195 ECBILT a coupled atmosphere ocean sea-ice model for climate predictability studies / R.J. Haarsma a.o.
196 Environmental and climatic consequences of aviation: final report of the KNMI contributions to the AERO-project / W. Wauben a.o.
197 Global radiation measurements in the operational KNMI meteorological network: effects of pollution and ventilation / F. Kuik
198 KALCORR: a kalman-correction model for real-time road surface temperature forecasting / A. Jacobs
199 Macroseismische waarnemingen Roswinkel 19-2-1997 / B. Dost e.a.
200 Operationele UV-metingen bij het KNMI / F. Kuik
201 Vergelijking van de Vaisala's HMP233 en HMP243 relatieve luchtvochtigheidsmeters / F. Kuik
202 Statistical guidance for the North Sea / Janet Wijngaard and Kees Kok
203 UV-intercomparison SUSPEN / Foeke Kuik and Wiel Wauben
204 Temperature corrections on radiation measurements using Modtran 3 / D.A. Bunskoek, A.C.A.P. van Lammeren and A.J. Feijt
205 Seismisch risico in Noord-Nederland / Th. De Crook, H.W. Haak en B. Dost
206 The HIRLAM-STAT-archive and its application programs / Albert Jacobs
207 Retrieval of aerosol properties from multispectral direct sun measurements / O.P. Hasekamp
208 The KNMI Garderen Experiment, micro-meteorological observations 1988-1989; instruments and data / F.C. Bosveld a.o.
209 CO2 in water and air during ASGAMAGE: concentration measurements and consensus data / Cor M.J. Jacobs, Gerard J. Kunz, Detlev Sprung a.o.
210 Elf jaar Cabauw-metingen / J.G. van der Vliet
211 Indices die de variabiliteit en de extremen van het klimaat beschrijven / E.J. Klok
212 First guess TAF-FGTAF: semi-automation in TAF production / Albert Jacobs
213 Zeer korte termijn bewolkingsverwachting met behulp van METCAST: een verificatie en beschrijving model-uitvoer / S.H. van der Veen
214 The implementation of two mixed-layer schemes in the HOPE ocean general circulation model / M. van Eijk
215 Stratosphere-troposphere exchange of ozone, diagnosed from an ECMWF ozone simulation experiment / Harm Luykx
216 Evaluatierapport Automatisering Visuele Waarnemingen Ontwikkeling Meestsystemen / Wiel Wauben en Hans de Jongh
217 Verificatie TAF en TREND / Hans van Bruggen
218 LEO - LSG and ECBILT coupled through OASIS: description and manual/A. Sterl
219 De invloed van de grondwaterstand, wind, temperatuur en dauwpunt op de vorming van stralingsmist: een kwantitatieve benadering / Jan Terpstra
220 Back-up modellering van windmeetmasten op luchthavens / Ilja Smits
221 PV-mixing around the tropopause in an extratropical cyclone / M. Sigmond
222 NPK-TIG oefendag 16 december 1998 / G.T. Geertsema, H. van Dorp e.a.
223 Golfhoogteverwachtingen voor de Zuidelijke Noordzee: een korte vergelijking van het ECMWF-golfmodel (EPS en operationeel), de nautische gidsverwachting, Nedwam en meteoroloog / D.H.P. Vogelezang en C.J. Kok.
224 HDFg library and some HDF utilities: an extention to the NCSA HDF library user's manual & reference guide / Han The

▼ WETENSCHAPPELIJK RAPPORT = SCIENTIFIC REPORT (WR)

96-01 A new algorithm for total ozone retrieval from direct sun measurements with a filter instrument / W.M.F. Wauben
96-02 Chaos and coupling: a coupled atmosphere ocean-boxmodel for coupled behaviour studies / G. Zondervan
96-03 An acoustical array for subsonic signals / H.W. Haak
96-04 Transformation of wind in the coastal zone / V.N. Kudryavtsev a.o.
96-05 Simulations of the response of the ocean waves in the North Atlantic and North Sea to CO2 doubling in the atmosphere / K. Rider a.o.
96-06 Microbarograph systems for the infrasonic detection of nuclear explosions / H.W. Haak and G.J. de Wilde
96-07 An ozone climatology based on ozonesonde measurements / J.P.F Fortuin
96-08 GOME validation at KNMI and collaborating institutes / ed. P. Stammes a.o.
97-01 The adjoint of the WAM model / H. Hersbach
97-02 Optimal interpolation of partitions: a data assimilation scheme for NEDWAM-4; description and evaluation of the period November 1995 - October 1996 / A.Voorrips
97-03 SATVIEW: a semi-physical scatterometer algorithm / J.A.M. Janssen a.o.
97-04 GPS water vapour meteorology . status report / H. Derks a.o.
97-05 Climatological spinup of the ECBILT oceanmodel / Arie Kattenberg a.o.
97-06 Direct determination of the air-sea transfer velocity of CO2 during ASGAMAGE / J.C.M. Jacobs, W. Kohsiek and W.A. Oost
97-07 Scattering matrices of ice crystals / M. Hess, P. Stammes a.o.
97-08 Experiments with horizontal diffusion and advection in a nested fine mesh mesoscale model / E.I.F. de Bruijn
97-09 On the assimilation of ozone into an atmospheric model / E.Valur Hólm
98-01 Steady state analysis of a coupled atmosphere ocean-boxmodel / F.A. Bakker
98-02 The ASGAMAGE workshop, September 22-25, 1997 / ed. W.A. Oost
98-03 Experimenting with a similarity measure for atmospheric flows / R.A. Pasmanter and X.-L. Wang
98-04 Evaluation of a radio interferometry lightning positioning system / H.R.A. Wessels
98-05 Literature study of climate effects of contrails caused by aircraft emissions / V.E. Pultau
99-01 Enhancement of solar and ultraviolet surface irradiance under partial cloudy conditions / Serdal Tunç
99-02 Turbulent air flow over sea waves: simplified model for applications / V.N. Kudryavtsev, V.K. Makin and J.F. Meirink
99-03 The KNMI Garderen experiment, micro-meteorological observations 1988-1989: corrections / Fred C. Bosveld
99-04 ASGAMAGE: the ASGASEX MAGE experiment . final report / ed. W.A.Oost
2000-01 A model of wind transformation over water-land surfaces / V.N. Kudryavtsev, V.K. Makin, A.M.G. Klein Tank and J.W Verkaik